Morphology and Microphase Separation of Star Copolymers

Jicheol Park, Sangshin Jang, Jin Kon Kim

National Creative Research Initiative Center for Smart Block Copolymers, Department of Chemical Engineering, Pohang University of Science and Technology, Pohang, Kyungbuk 790-784, Republic of Korea
Correspondence to: J. K. Kim (E-mail: jkkim@postech.ac.kr)

Received 24 July 2014; accepted 3 September 2014; published online 8 October 2014
DOI: 10.1002/polb.23604

ABSTRACT: Star copolymers have attracted significant interest due to their different characteristics compared with diblock copolymers, including higher critical micelle concentration, lower viscosity, unique spatial shape, or morphologies. Development of synthetic skills such as anionic polymerization and controlled radical polymerization have made it possible to make diverse architectures of polymers. Depending on the molecular architecture of the copolymer, numerous morphologies are possible, for instance, Archimedean tiling patterns and cylindrical microdomains at symmetric volume fraction for miktoarm star copolymers as well as asymmetric lamellar microdomains for star-shaped copolymers, which have not been reported for linear block copolymers. In this review, we focus on morphologies and microphase separations of miktoarm (A_mB_n and ABC miktoarm) star copolymers and star-shaped [(A-*b*-B)$_n$] copolymers with nonlinear architecture. © 2014 Wiley Periodicals, Inc. J. Polym. Sci., Part B: Polym. Phys. **2015**, *53*, 1–21

KEYWORDS: block copolymers; morphology; phase behavior; phase transition

INTRODUCTION Block copolymers have been extensively investigated because of their diverse self-assembled structures such as spheres, cylinders, gyroids, and lamellae depending on the volume fraction of one of the blocks (f), the degree of polymerization (N), the Flory-Huggins interaction parameter (χ), and the molecular architecture of the block copolymers.[1–4] These nanostructures have been widely used for various applications such as templates, membranes, optical materials, and data storage media.[5–15]

Compared with linear diblock copolymers, diverse architectures of copolymers such as miktoarm star copolymers or star-shaped copolymers have been explored because of the expectation of different morphologies or physical properties induced by different molecular architecture. For example, unimolecular micelles composed of star-shaped copolymers showed much higher stability than the micelles made of diblock copolymers because the arms of star-shaped copolymers are covalently linked to the core.[16–18] Lin and coworkers[19–22] used very stable unimolecular micelles made of star-shaped copolymers for the fabrication of monodisperse colloidal nanocrystals.

Development of synthetic skills such as anionic polymerization and controlled radical polymerization (CRP) has made it possible to make diverse architectures of polymers using arm-first or core-first method. Linking preformed living polymers to the core by coupling or crosslinking is an arm-first method,[23–25] while polymerization of polymers from macroinitiator with known number of initiating sites is a core-first method.[26–28] Since excellent reviews on synthesis and properties of star polymers have been available,[29–32] this review is mainly focused on morphologies and microphase separations of miktoarm (A_mB_n and ABC miktoarm) star copolymers and star-shaped [(A-*b*-B)$_n$] copolymers with nonlinear architecture.

Miktoarm star copolymers consist of heteroarms emanating from a central core with different chemical compositions or molecular weights (A_mB_n : miktoarm star copolymer with m arms of A homopolymer and n arms of B homopolymer), while star-shaped copolymers contain block copolymer homoarms with identical chemical compositions [(A-*b*-B)$_n$: star-shaped copolymer with n arms of A-*b*-B diblock copolymer. Here the first written A block represents the inner block (core) and B block is the outer block (shell) of star-shaped copolymer], as shown in Scheme 1. Morphologies or microphase separations of linear diblock copolymers are decided by the volume fraction of one of the blocks. For example, spherical or cylindrical microdomains are only observed at asymmetric volume fractions, while lamellar microdomains are shown at symmetric volume fractions in diblock copolymers. However, nonlinear block copolymers showed cylindrical microdomains even at symmetric volume

Jicheol Park is a Ph. D. candidate in the Department of Chemical Engineering of Pohang University of Science and Technology (POSTECH) under the supervision of Prof. Jin Kon Kim. His research interests include the effect of macromolecular architecture on self-assembly of block copolymers.

Sangshin Jang is a Ph. D. candidate in the Department of Chemical Engineering of POSTECH under the supervision of Prof. Jin Kon Kim. His research interests include self-assembly of star-shaped block copolymers.

Jin Kon Kim is a POSTECH fellow and a full professor of Chemical Engineering of POSTECH. Also, he is the director of the Center for Smart Block Copolymer Self-Assembly funded by the National Creativity Research Initiative Program supported by National Research Foundation in Korea. He received his B.S. (1980) from Seoul National University (Korea) in Chemical Engineering and M.S. (1982) from Korea Advanced Institute of Science and Technology (Korea) in Chemical Engineering, and Ph.D. (1990) from Polytechnic University in Chemical Engineering. He was a senior research scientist at Polymer Research Institute of LG Chem. Co. in Korea. His research interests include phase behavior and phase transition of block copolymers, development of new functional nanomaterials for membranes and photovoltaic cells, interfacial properties and interfacial tension measurement of reactive polymer blends and nanocomposites containing polymer blends and organoclays.

fraction due to the molecular architecture. In addition, they exhibited Archimedean tiling patterns[33–35] that have not been reported for linear block copolymers.

MORPHOLOGIES AND MICROPHASE SEPARATIONS OF MIKTOARM STAR COPOLYMERS

Theory

The effect of macromolecular architecture on microstructure of miktoarm star copolymers has been extensively investigated theoretically and experimentally. Milner[36] was the first to theoretically obtain the phase diagram for A_nB_n miktoarm star copolymer. He assumed that miktoarm star copolymers lied in strong segregation limit in which the interface between two blocks is sharp. The morphologies of microstructure are determined by the competition between the increase of stretching free energy as the each arm stretches away from the interface and the reduction of interfacial tension.

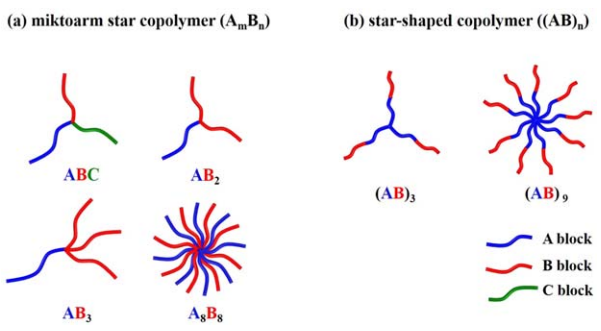

SCHEME 1 Schematic architectures of (a) miktoarm star copolymers (A_mB_n) and (b) star-shaped copolymers ($(A\text{-}b\text{-}B)_n$).

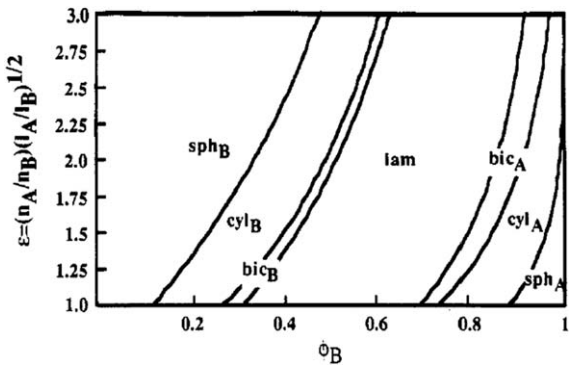

FIGURE 1 Phase diagram in the strong segregation limit for miktoarm star copolymers as a function of volume fraction of the B monomer. (Reproduced from ref. 36, with permission from American Chemical Society.)

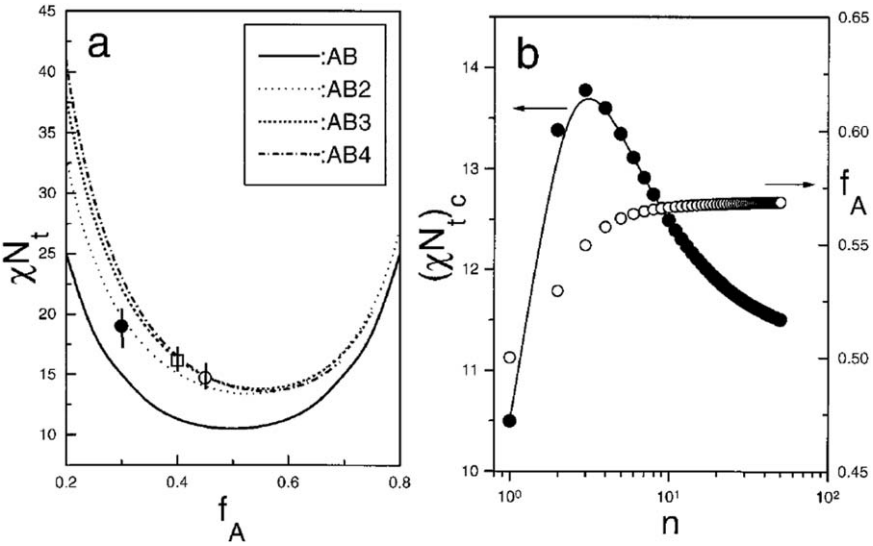

FIGURE 2 (a) The spinodal curves (χN_t vs. f_A) for diblock and AB_n miktoarm star copolymers with three different values of n (2, 3, and 4). The experimental results obtained from an AB_2 (•) and two AB_3 (□, ○) miktoarm star copolymers are shown together with the investigated temperature range (vertical lines). (b) Critical values of χN_t plotted as a function of the number of arms of the B blocks. The dependence of the optimal composition corresponding to the minima of the spinodal curves is also shown. (Reproduced from ref. 37, with permission from American Chemical Society.)

Figure 1 shows the phase diagram for miktoarm star copolymers as function of volume fraction of B (ϕ_B). With increasing asymmetric parameter $\varepsilon \equiv (n_A/n_B)(l_A/l_B)^{1/2}$, where n_A, n_B are the numbers of A and B blocks, and l_A, l_B are characteristic lengths of A and B, respectively, the phase boundary between microdomains moved toward ϕ_B.

Floudas et al.[37] predicted microphase separation for diblock and AB_n miktoarm star copolymer based on the mean field theory. Spinodal curves were calculated for the AB_n miktoarm star copolymers with n up to 100 [Fig. 2(a)]. Microphase separation for AB_n miktoarm star copolymers becomes more difficult than that of linear diblock copolymers, because the critical value of the χN_t ($N_t = N_a + nN_b$) of AB_n miktoarm star copolymers is higher than that of diblock copolymers [Fig. 2(b)]. In addition, the spinodal curves are asymmetric against one of the volume fractions due to the asymmetry of miktoarm star copolymers. Interestingly, the maximum critical value of χN_t in AB_n miktoarm star copolymers appeared at $n = 3$ because of delicate balance between the stretching free energies of A and B arms. The theoretical predictions on phase boundaries are consistent with experimentally measured ones by small angle X-ray scattering (SAXS) method for AB_3 miktoarm star copolymers composed of one arm of PS and three arms of PI.

Grason and Kamien[38] obtained phase behavior of AB_n miktoarm star copolymers in the strong segregation limit, using self-consistent field theory (SCFT) analysis (Fig. 3). All phase diagrams are not symmetric, which means that the shape of interfaces is curved toward the A block because of asymmetry of molecular architecture. They found that the interface between two blocks is highly distorted when the number of B arms is higher than 3. As a result, increasing the number of B arms enhances the stability of A15 phase (sphere-like micelles) which is not observed for linear diblock copolymer (Fig. 3). Later, Matsen[39] calculated the phase diagram for AB_2 miktoarm star copolymer and found perforated lamellae (PL) and *Fddd* (O^{70}, orthorhombic and single-network structure)[40] phases near gyroid phase (Fig. 4).

Dissipative particle dynamics were also applied to study microphase separation of AB_2 miktoarm star copolymers, where hydrodynamic interaction and fluctuation were considered.[41] The phase diagram obtained by the dissipative particle dynamics is in good agreement with that predicted by SCFT. However, in contrast to the prediction based on SCFT, AB_2 miktoarm star copolymers with small volume fractions of B block do not form the ordered structure, but only a tube-like phase appears. These results are often observed in experiments because dissipative particle dynamics considered the possibility of aggregates.

Interesting category of miktoarm star copolymer is ABC miktoarm star terpolymer consisting of three chemically different arms [Fig. 1(a)]. Since the molecular architecture of ABC miktoarm star terpolymers with the immiscible arms connected at a single point affects significantly the microphase separation, new kinds of morphologies including quasicrystalline tiling pattern that could not be attained by linear block copolymers are observed for nonlinear block copolymers.[34] This is because the single junction point of ABC miktoarm star terpolymers is located on the lines where three kinds of the interfaces meet together if the interaction parameters between arms are strong enough (Fig. 5). Gemma et al.[43] obtained the phase diagram of ABC miktoarm star terpolymers based on Monte Carlo simulation method. They assumed that the miktoarm star copolymers lay in strong segregation limit and the interaction parameters

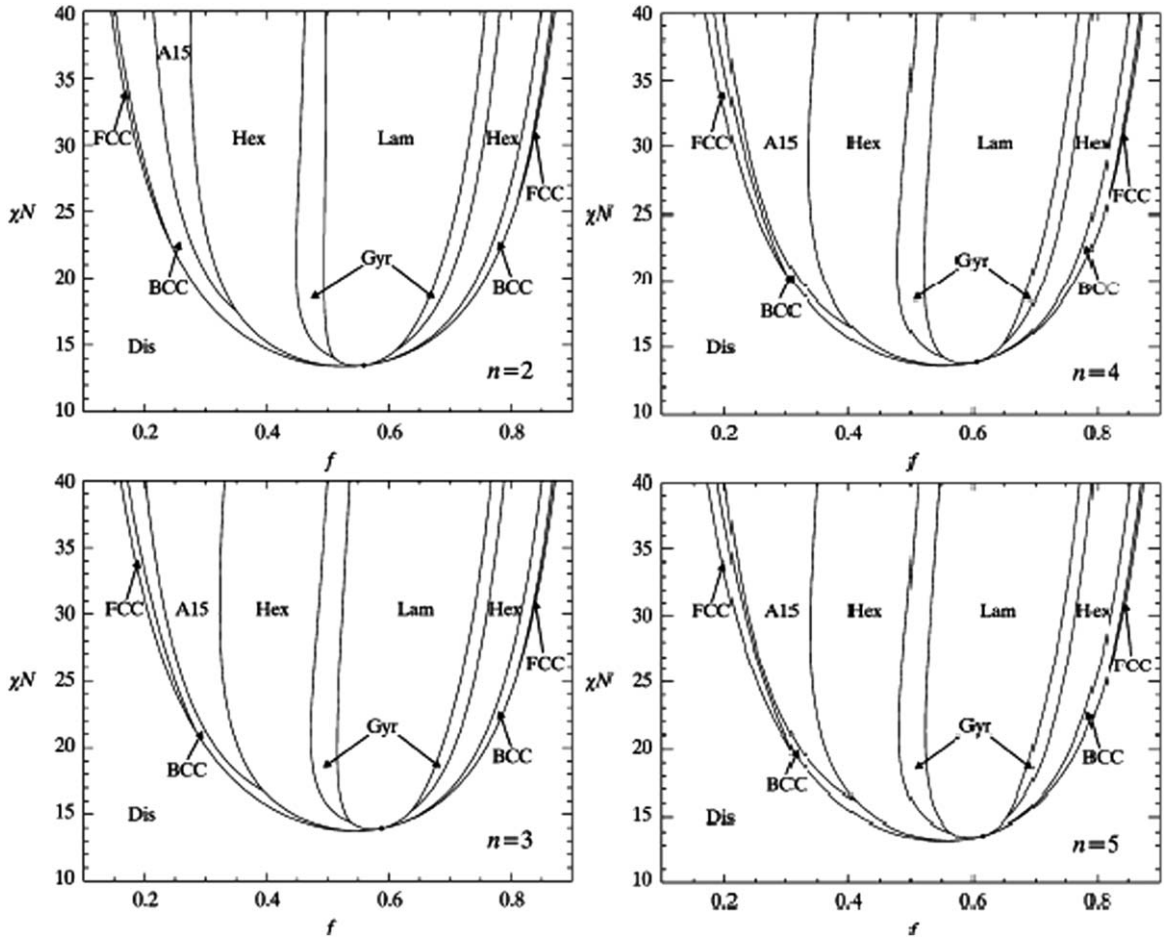

FIGURE 3 Theoretical phase diagram of AB_n miktoarm star copolymers for $n = 2$, 3, 4, and 5 calculated using SCFT. Dis labels regions where the melt is disordered. Stable regions of ordered phases are labeled: (Lam) lamellar; (Gyr) gyroid, $Ia\bar{3}d$ symmetry; (Hex) hexagonal-columnar, *p6mm* symmetry; A15 sphere phase, $Pm\bar{3}n$ symmetry; (BCC) body-centered-cubic lattice of spheres, $Im\bar{3}m$ symmetry; and (FCC) face-centered cubic lattice of spheres, $Fm\bar{3}m$ symmetry. (Reproduced from ref. 38, with permission from American Chemical Society.)

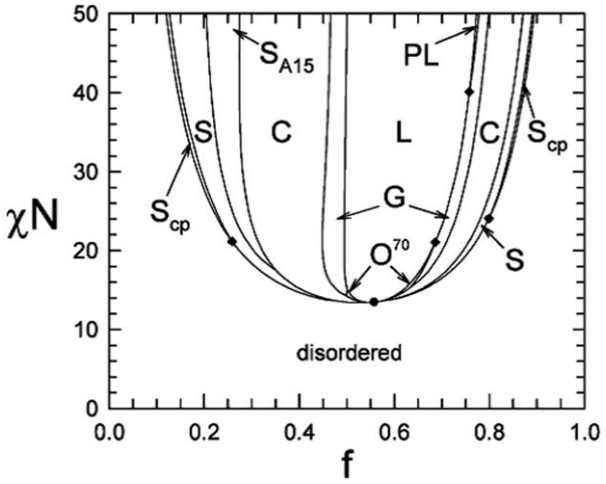

FIGURE 4 Theoretical phase diagram of AB_2 miktoarm star copolymers. PL, *Fddd* are additionally shown compared to Figure 3. (Reproduced from ref. 39, with permission from American Chemical Society.)

between three blocks are equal. The predicted phase diagram of the ABC miktoarm star terpolymer is shown in Figure 6, where arm-length ratio is N_a:N_b:N_c = 1:1:*x*. Conversely, Pan and coworkers[44] focused on the localization of junction point of the ABC miktoarm star terpolymers using dynamic density functional theory. When the miscibility of one block with the other two blocks increased, the junction points were distributed over the intermaterial dividing surfaces, not lines. This means that the interaction parameters between arms also play an important role in determining microdomains and the location of junction points.

Later, Birshtein et al.[45] developed a theory to predict lamellar morphology of ABC miktoarm star terpolymer with interaction parameters with $\chi_{AB} \gg \chi_{AC} = \chi_{BC}$. In this case, A and B microdomains are separated by the C microdomain, where small parts of A and B chains are located in the C domain because of the junction point of three arms (Fig. 7). Stretching of A and B chains in the mixed C domain and compression of the C chains occur because unfavorable A/C and B/C interactions should be minimized (Fig. 7).

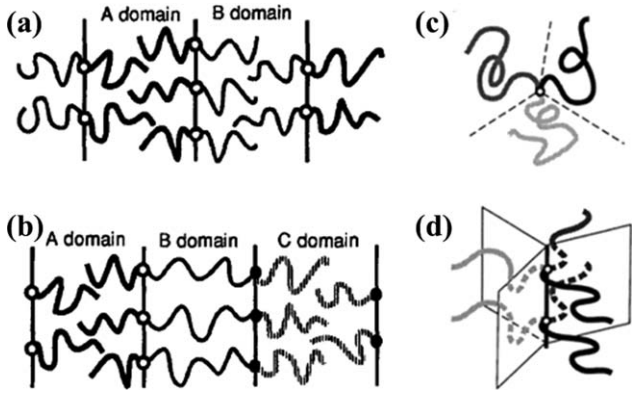

FIGURE 5 Schematic illustrations of copolymer chains. (a) AB diblock copolymers: the chemical junction points are confined at the interfaces; (b) linear ABC triblock copolymers: the chemical junction points are confined at the interfaces. (Reproduced from ref. 42, with permission from Elsevier). (c) ABC miktoarm star terpolymers consisting of three different arms. Between three arms, three interfaces appear, (d) Junction point line. Junction point depicted by small circles must gather on a line where three interfaces meet. The chemical junction points are confined on a line. (Reproduced from ref. 40, with permission from American Chemical Society.)

Dissipative particle dynamics were also applied to study phase behavior of ABC miktoarm star terpolymers.[47] Figure 8 shows phase diagram of ABC miktoarm star terpolymer with dimensionless interaction parameters $\alpha_{AB} = \alpha_{AB} = \alpha = 36$ ($\alpha_{IJ}(T) = \alpha_{II} + 3.497\chi_{AB}(T)$, I,J = A, B, C. The degree of polymerization for the ABC miktoarm star terpolymer is fixed at $N = N_A + N_B + N_C = 20$. When one of the three arms is a minor block which cannot self-assemble to form one microdomain, the phase behavior is similar to that of linear diblock copolymers. When three arms have comparable volume fractions, three-phase polygonal morphologies, [6.6.6], [8.8.4], [10.6.4;10.8.4] [3.3.4.3.4], [10.6.6;10.6.4], are formed. The polygonal morphology is mainly determined by the volume fraction of three arms but not by the interaction parameters.

There are few theoretical studies for the phase behavior (or microphase separation) of rod-like (or rigid) block-containing miktoarm star copolymers. In this situation, the self-assembly of miktoarm star copolymers is influenced not only by the incompatibility between rod-like blocks and flexible blocks but also by the tendency of the rod-like block to form orientational order. Xia et al.[48] studied the phase diagram of $(coil)_2$rod miktoarm star copolymers and linear rod-*b*-coil diblock copolymers based on SCFT (Fig. 9). Though the phase diagrams of two cases are similar, one particular exception is observed. When the volume fraction of rod block was 0.45, the cylindrical morphology was formed for miktoarm star copolymer, while the perforated lamellar morphology was formed for the corresponding linear rod-*b*-coil diblock copolymer. This is caused by the interplay between the interfacial energy and elastic stretching free energy of the coil block. They also found that the phase diagram of T-shaped rod-coil block copolymers was also different from corresponding linear diblock copolymers and $(coil)_2$rod miktoarm star copolymers.[49] This is due to the steric hindrance attributed by the anchored coil blocks which affect self-assembly of block copolymers.

The theories for phase behavior of miktoarm star copolymers consisting of all coil blocks have been well-developed and experimental results are mostly in good agreement with theoretical prediction. Many theoretical studies have been performed on rod-coil linear block copolymers considering the Maier–Saupe interaction and the stiffness of rod block in addition to conventionally used the volume fraction and the Flory–Huggins interaction.[50,51] In contrast, the theories for rod-containing miktoarm star copolymer are very few,[48]which makes difficult to predict phase behavior before the experiments. Therefore, it is essential to develop theories of rigid-containing miktoarm star copolymer

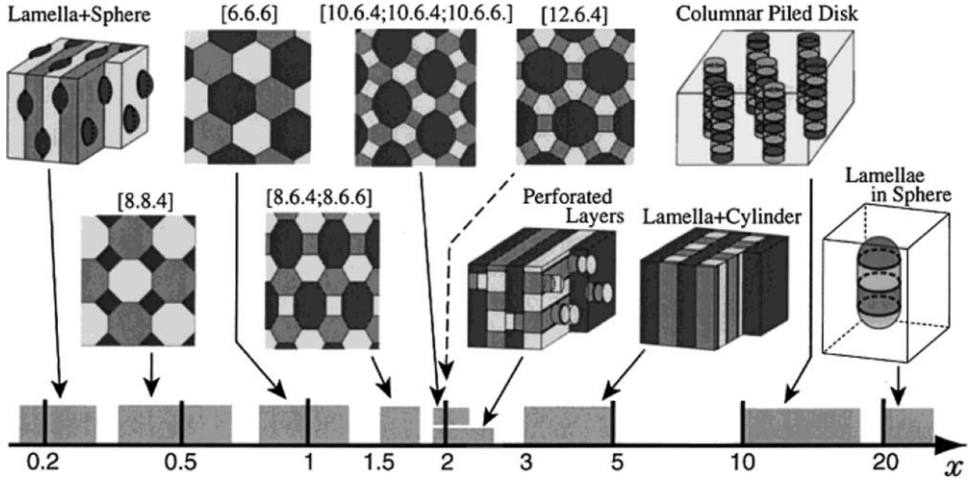

FIGURE 6 Theoretical phase diagram of ABC miktoarm star terpolymers with arm-length ratio 1:1:*x* and symmetric interactions between three components. A (light gray), B (medium gray), and C (dark gray) are displayed. Morphologies are lamella + sphere (L + S), five cylindrical structures in sectional view denoted by polygons around a vertex in the sections, perforated layer, lamellar + cylinder (L + C), columnar piled disk, and lamella-in-sphere. (Reproduced from ref. 44, with permission from American Institute of Physics.)

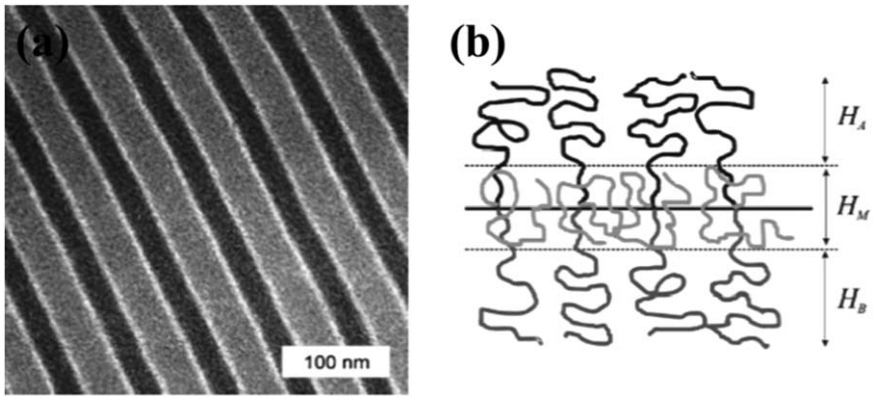

FIGURE 7 Lamellar morphology of ABC miktoarm star terpolymer: (a) TEM micrograph[46] for (PS)(PB)(P2VP) miktoarm star terpolymer with arm-length ratio 14:37:49 (Reproduced from ref. 46, with permission from American Chemical Society) and (b) schematic representation. (Reproduced from ref. 45, with permission from John Wiley and Sons.)

to understand the phase behavior and find useful microstructures for potential applications.

Experimental of Miktoarm Star Copolymers

A_mB_n Miktoarm Star Copolymer

Hadjichristidis and coworkers[52,53] studied microphase separation of $PS(PI)_2$ miktoarm star copolymers. They found that

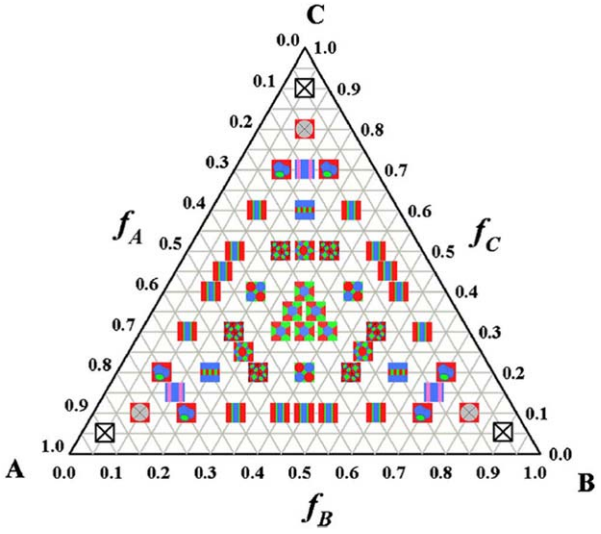

FIGURE 8 Theoretical phase triangle of ABC miktoarm star terpolymer calculated using dissipative particle dynamics with $\alpha_{AB} = \alpha_{AB} = \alpha_{AC} = 36$ ($N = N_A + N_B + N_C = 20$). In the figure, ( ) [6.6.6]; ( ) [8.8.4]; ( ) [10.6.4;10.8.4] (3.3.4.3.4); ( ) [10.6.6;10.6.4]; ( ) $C_I + C_J$ within L (*I* and *J* are minority components); ( ) $L_{I,J}$ with *K* in the interfaces (*I* and *J* are majority components); ( ) *I*- and *J*-segregated domains within L (*I* and *J* are minority components); ( ) gyroid; ( ) *IJ*-formed tubes (*I* and *J* are minority components); ( ) disorder. (Reproduced from ref. 47, with permission from American Physical Society).

$(PS)(PI)_2$ miktoarm star copolymer with 40 vol % PS shows hexagonally packed cylinder (HEX) of PS. This result is in contrast to linear diblock copolymer of the same composition which showed lamellar morphology. Tselikas et al.[54] showed that the boundary between two microdomains for $(PS)(PI)_2$ miktoarm star copolymers is shifted toward higher PS volume fraction compared with linear PI-*b*-PS diblock copolymers (Fig. 10). Interestingly, $(PS)(PI)_2$ miktoarm star copolymer with 53 vol % of PS has a bicontinuous cubic morphology.[55] A randomly oriented worm micelle morphology was observed in $(PS)(PI)_2$ miktoarm star copolymer with 81 vol % of PS. This morphology only occurs near the particular volume fraction where two PI chains per molecule are first forced to the concave side of the interface. At this unique volume fraction, the novel miktoarm architecture frustrated the system from choosing a lattice during microphase separation.[56]

Later, $(PS)(PI)_3$ miktoarm star copolymers were also synthesized and their phase behavior was studied.[57] The boundary between two microdomains for $(PS)(PI)_3$ miktoarm star copolymers was more shifted to higher PS volume fraction. The extent of the phase boundary shift increases with increasing the number of PI arms because of higher curvature of the PS/PI interphase that is curved toward the PS due to the overcrowding of PI. Interestingly, an unusual broken chevron tilt grain boundary was observed in $(PS)(PI)_5$ miktoarm star copolymer with 58 vol % of PS (Fig. 11). This new microstructure is attributed to interfacial bending resulting from architectural asymmetry of $(PS)(PI)_5$ miktoarm star copolymer which has extraordinarily large geometric packing constraints.[58]

Mavroudis et al.[59] investigated the phase behavior of $PS(P2MP)_3$ miktoarm star copolymers [here, P2MP is poly(2-methyl-1,3-pentadiene)]. The morphology of $PS(P2MP)_3$ miktoarm star copolymers is quite different from $PI(PI)_3$ miktoarm star copolymer even though P2MP has only one extra methyl group. $PS(P2MP)_3$ miktoarm star copolymers with 74 vol % of PS formed a biphasic structure of 1D-lamellar and 3D-double gyroid structure, which is not predicted by the

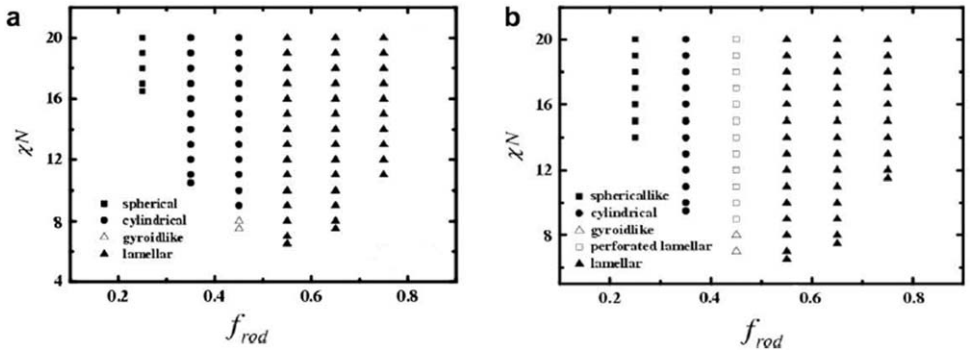

FIGURE 9 Theoretical phase diagram of (a) $(rod)_2coil$ miktoarm star copolymer and (b) rod-coil linear diblock copolymer. (Reproduced from ref. 48, with permission from Elsevier.)

Milner's theory. The disagreement might be due to large differences in characteristic ratio (C_{oo}) and glass transition temperature (T_g) between P2MP and PI.

Recently, morphologies of AB_2, AB_3 miktoarm star copolymers composed of maltoheptaose block (A block) and PCL block (B block) were studied.[60] The AB_2 and AB_3 miktoarm star copolymers with 18 vol %, 9 vol % of A block showed body-centered cubic spheres (BCC) morphologies (Fig. 12). Interestingly, d-spacing of the BCC microstructures in the miktoarm star copolymers decreased as the arm number of the PCL blocks increased. Sub-10 nm BCC microdomain was obtained because of high interaction parameter between two blocks as well as molecular architecture. In contrast, A_2B miktoarm star copolymer with 16 vol % of A block produced a lamella morphology despite the low volume fraction.[61] This morphology resulted from lower curvature at interface because of molecular architecture.

The microstructures of PS_8PI_8 miktoarm star copolymers were investigated by Hadjichristidis and coworkers.[42,62] All of three $(PS)_8(PI)_8$ miktoarm star copolymer with 37, 44, and 47 vol % of PS and total molecular weight ranging from 330,000 to 894,000 formed lamellar morphologies. In agreement with the theory, $(PS)_8(PI)_8$ miktoarm star copolymer behaved similarly to linear diblock copolymers with the same composition. Turner et al.[63] investigated PS_2PB_2 miktoarm star copolymer. The lamellar spacing for symmetric PS-*b*-PB diblock copolymer is smaller than that for $(PS)_2(PB)_2$ miktoarm star copolymer, and the interfacial area per molecule for $(PS)_2(PB)_2$ miktoarm star copolymer is similar to that for $(PS)_8(PI)_8$ miktoarm star copolymer.[62]

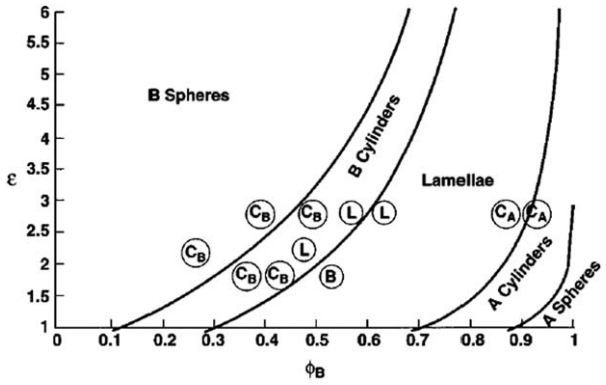

FIGURE 10 Comparison of observed morphologies with predictions of Milner.[36] Lines indicate the predicted boundaries between various morphologies. Letters indicate observed morphologies: C_B=cylinders of B, B=bicontinuous, L=lamellar, C_A=cylinders of A. (Reproduced from ref. 54, with permission from American Institute of Physics.)

Beyer et al.[64] investigated the morphologies of $(PS)_2(PB)_2$ miktoarm star copolymers using transmission electron microscopy (TEM), SAXS, and SANS. Five samples with 14, 28, 35, 68, and 87 vol % of PS showed various morphologies depending on the volume fraction of PS. Because all of the copolymers are in the strong segregation regime, morphologies were predicted by the Milner's theory. $(PS)_2(PI)_2$ with 28 vol % of PS formed a cylindrical morphology, although lamellae were predicted. Sample with 58 vol % of PS exhibited a cylindrical morphology, while bicontinuous morphology is predicted. This is because bicontinuous morphology is unstable in the strong segregation regime as a result of increased packing frustration.[65] With increasing number of n in $(PS)_n(PI)_n$ miktoarm star copolymers, the lamellar domain spacing is also increased.[66] This is because each polymer segment near the junction adopts a stretched trajectory away from the center core to minimize chain crowding.

Very recently, self-assembled morphologies of $A_3B_3C_3$ miktoarm star copolymer composed of PS, PI, and poly(4-methoxystyrene) (PMOS) were investigated.[67] The volume fractions of the PS, PMOS, and PI were estimated to be 31.4, 29.4, and 39.2%, respectively. They found via grazing incidence X-ray scattering that the thin films have highly ordered, in-plane oriented hexagonal structure consisting of truncated PS cylinders and truncated PMOS triangular prisms in the PI matrix. More interestingly, this hexagonal structure undergoes a rotational transformation which produces a 30°-rotated hexagonal structure at temperatures above 190 °C.

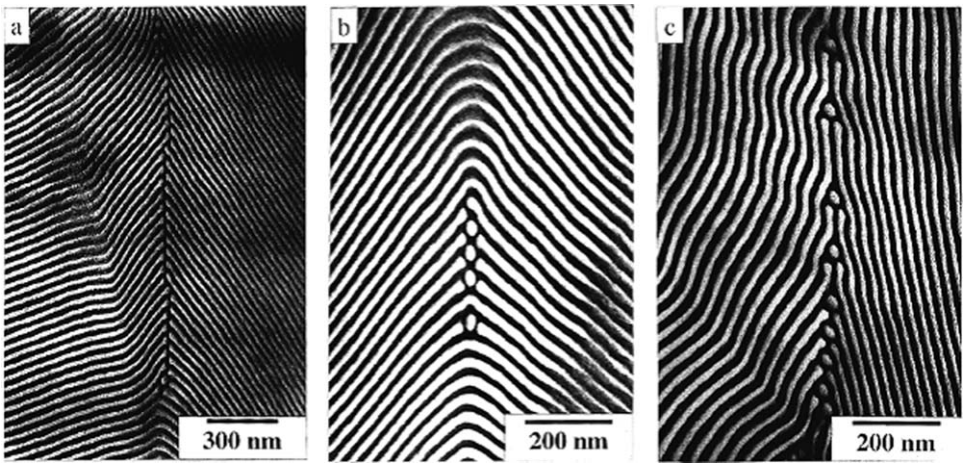

FIGURE 11 TEM micrograph of $(PS)(PI)_5$ miktoarm star copolymer with 58 vol % of PS symmetric tilt grain boundaries: (a) broken chevron, (b) broken chevron with cylinders, (c) broken Ω with cylinders. (Reproduced from ref. 58, with permission from American Chemical Society).

ABC Miktoarm Star Terpolymer

Compared to linear ABC triblock copolymer,[68] ABC miktoarm star terpolymer showed diverse morphologies. Hadijichristidis et al.[52] studied the morphology of ABC miktoarm star terpolymer, composed of PS, PI, and PB. Since PI and PB arms could be mixed due to small χN, (PS)(PI)(PB) miktoarm star terpolymer has similar morphologies of $(PS)(PI)_2$ miktoarm star copolymers.

Okamoto et al.[69] investigated, via differential scanning calorimeter, TEM, and SAXS, the phase behavior of ABC miktoarm star terpolymer composed of PS, PDMS, and poly(*tert*-butyl methacrylate) (PTBMA), each of them having similar weight fraction. Because three components are very incompatible, (PS)(PDMS)(PTBMA) miktoarm star terpolymer showed special microdomain not obtained by (PS)(PI)(PB) miktoarm star terpolymer. A miktoarm star terpolymer consisting of PS/PDMS/PBMA = 36/26/38 (wt %) shows a regular microdomain morphology with a threefold symmetry where each microdomain forms a 3D continuous network domain even though precise morphology is not conformed.

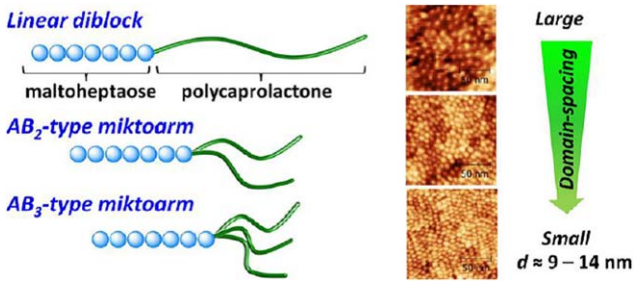

FIGURE 12 Schematic representation of linear diblock, AB_2 and AB_3 miktoarm star copolymer with the same composition and tapping mode AFM phase images for the thin films of each block copolymers. (Reproduced from ref. 60, with permission from American Chemical Society).

Sioula et al.[70] investigated the phase behavior of miktoarm terpolymer having PS, PI, and PMMA. PS and PMMA chains show a large incompatibility toward PI, whereas incompatibility between PS and PMMA is weak. All (PS)(PI)(PMMA) miktoarm star terpolymers showed three-microphase and 2D periodic microstructure of an inner PI column with a surrounding PS annulus in a matrix of PMMA. There is no interface between PI and PMMA, which means PMMA arms passed through the PS domain to reduce unfavorable contact between PI and PMMA. They found a new morphology for (PS)(PI)(PMMA) miktoarm star terpolymer having 38 vol % of PS, 28 vol % PI, and 34 vol % of PMMA. The PMMA domain was surrounded by alternating PI and PS microdomains, which forms hexagonal-shaped cylindrical columns with *p6mm* symmetry (Fig. 13).[71] This is a direct evidence that the junction is confined to the line where the three interfaces meet, and is attributed to nearly symmetric volume fractions of the three arms in (PS)(PI)(PMMA) miktoarm star terpolymers.

Yamauchi et al.[72] investigated the microdomain structure of ABC miktoarm star terpolymer composed of PS, PI, and PDMS using energy-filtering TEM (EF-TEM) together with 3D electron tomography. They prepared two samples for TEM. One is the sample without stain, and the other is sample stained with OsO_4. In both samples, only one phase has a contrast under TEM; thus, it is complicated to analyze the 3D microdomain structure. When energy-filtering TEM was used, complex macrodomain morphology with the coexistence of three different cylindrical structures was identified (Fig. 14).

(PS)(PB)(P2VP) miktoarm star terpolymers show various morphologies depending on the relative volume ratio of each block.[73] It shows tetragonal or distorted hexagonal

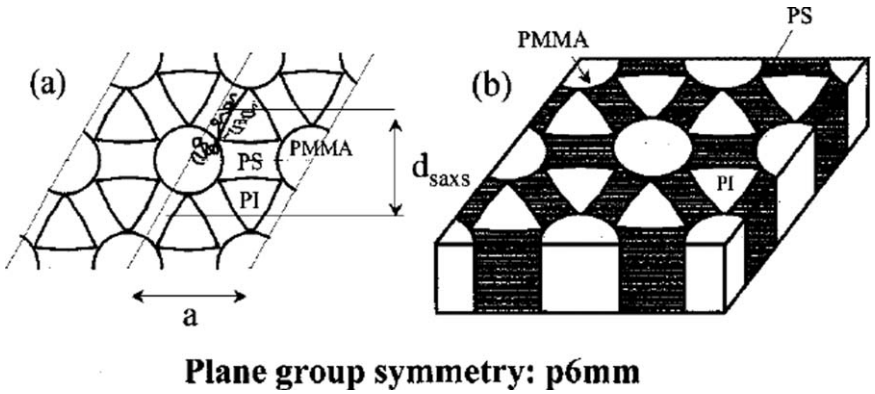

FIGURE 13 Schematic microdomain structure of the (PS)(PI)(PMMA) miktoarm star terpolymer with 38 vol % of PS, 28 vol % of PI, and 34 vol % of PMMA. The areas of each component are proportional to the volume fractions. (a) Representative chain conformation of a miktoarm star terpolymer and the location of the junction point are indicated. (b) Perspective showing the junction points residing at the vertexes where the three types of microdomains intersect. (Reproduced from ref. 71, with permission from American Chemical Society.)

morphologies when P2VP fraction is low. When the P2VP volume fraction was increased to 50–60 vol %, a hexagonal morphology was formed where the junction point is located along the line. Lamellar morphologies were formed when volume fraction of PB was larger than the volume fraction of PS even though the volume fraction of P2VP was varied. This is possible because the incompatibility between PB and P2VP is larger.

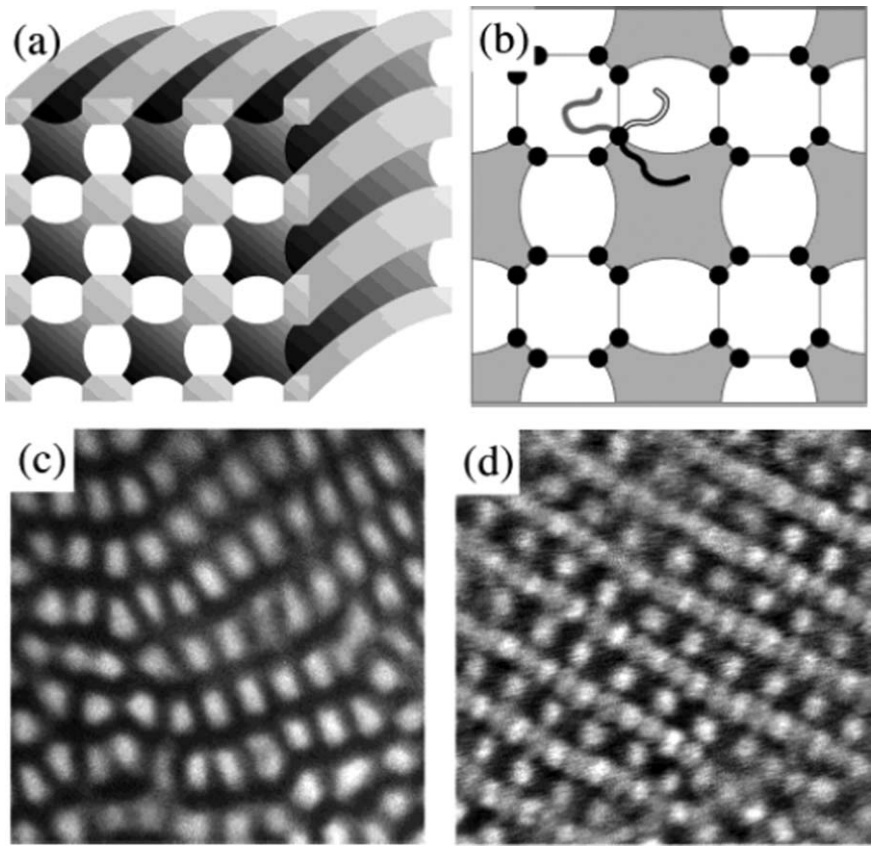

FIGURE 14 (a) Schematic illustration of the model for the microdomain structure of the (PI)(PS)(PMDS) miktoarm star terpolymer consisting of dark (PI), gray (PDMS), and bright (PS) cylinders with characteristic shapes. (b) A cross-sectional view of the cylinders in (a). The junction points of the miktoarm star are confined on the curved lines. (c) EF-TEM images of unstained (PI)(PS)(PMDS) miktoarm star terpolymer. (d) EF-TEM image of the OsO_4-stained sample. (Reproduced from ref. 72, with permission from American Chemical Society.)

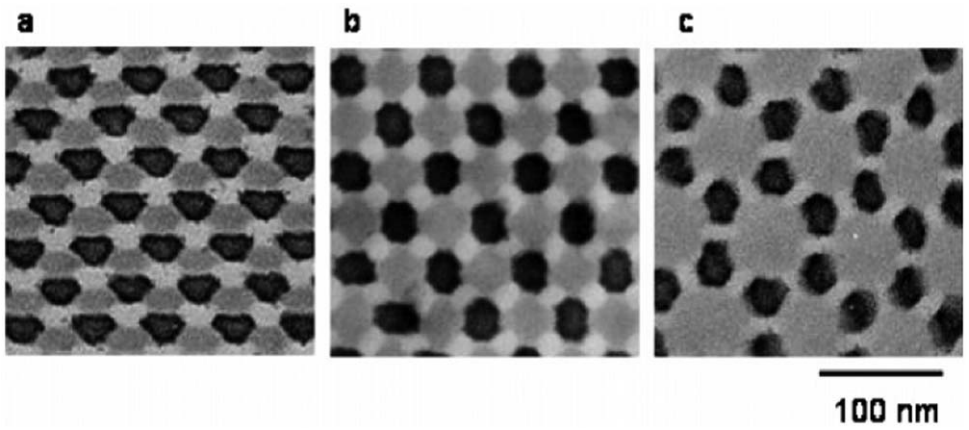

FIGURE 15 TEM images of ABC star block terpolymers composed of PS, PI, and P2VP, which have different volume ratio. (a) volume ratio of PS:PI:P2VP are 1:1:0.7, (b) volume ratio of PS:PI:P2VP are 1:1:1.2, and (c) volume ratio of PS:PI:P2VP are 1:1:0.7. (Reproduced from ref. 74, with permission from American Chemical Society.)

Matsushita and coworkers[74–76] made a significant contribution to microphase separation of ABC miktoarm star terpolymers. They prepared (PS)(PI)(P2VP) miktoarm terpolymers with volume ratios of PS:PI:P2VP having 1:1:0.7, 1:1:1.2, and 1:1:1.9. All of the samples formed three-phase microdomain structures (Fig. 15). Honeycomb-type structure where three different microdomains form mutually hexagonal domain was observed for the first time. However, each microdomain morphology has many defects compared to linear copolymers due to the difference in times for structural formation between ABC miktoarm star terpolymers and linear diblock copolymers. The junction point of linear diblock copolymer can move 2D during the formation of microphases, while the junction point of ABC miktoarm star terpolymer move 1D (Fig. 16). This different mobility of connecting point makes linear diblock copolymer attain a more stable structure than ABC miktoarm star terpolymer. They also used microbeam SAXS patterns, whose results are consistent with those obtained by TEM, and the lattices formed by (PS)(PI)(P2VP) miktoarm star terpolymer are distorted in comparison with the ideal lattice.[77]

Interesting morphologies were discovered in (PS)(PI)(P2VP) miktoarm star terpolymers whose volume ratios of PS:PI:P2VP are $1.0:1.8:X$ $(4.3 \leq X \leq 53)$.[78] Depending on the range of X, three kinds of hierarchical morphologies, cylinders-in-lamella $(4.3 \leq X \leq 11)$, lamellae-in-cylinder $(12 \leq X \leq 32)$, and lamellae-in sphere structure $(X = 53)$ are formed. In the cylinders-in-lamella morphology, PI and PS chain consists of cylindrical PI domains in matrix of PS. This combined layer constitutes an alternating lamellar morphology with layers of PS domains (Fig. 17). Several kinds of structure-in-structure morphology already have been reported.[79,80] However, hierarchical morphology consisting of cylinders in lamellar structure were reported for the first time in this work, which is contrast to previously reported hierarchical morphology of smaller lamellae in another large-sized lamellar structure.[81,82]

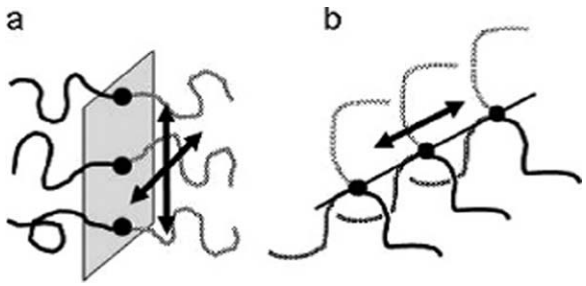

FIGURE 16 Schematic drawings of mobility of connecting points of (a) AB diblock copolymers and (b) ABC miktoarm star terpolymers. (Reproduced from ref. 74, with permission from American Chemical Society.)

Recently, Matsushita et al.[33] reported various morphologies using (PS)(PI)(P2VP) miktoarm star terpolymers with different volume ratios between the arms (Fig. 18). When asymmetry in volume ratio between the arms was increased, a four-branched zinc-blende type morphology was created. This network structure has seldom been observed for the polymer. They explained that the formation of peculiar structure is because the repulsion force between PI and P2VP is the strongest, resulting in reduced contact area between PI and P2VP microdomain. In addition, (PS)(PI)(P2VP) miktoarm star terpolymers are in the frustrated state in bulk, which makes their junction point have to be aligned along a 1D line. Further increase of the asymmetry created hyperbolic tiling on a gyroid membrane. This structure is also interesting because the major component forms a double network and the minor one forms gyroid membranes, in contrast to the usual expectation that minor component forms double networks in block copolymer systems. More interestingly, Hayashida et al.[34] observed quasicrystalline tiling pattern with 12-fold symmetry in a (PS)(PI)(P2VP) miktoarm star terpolymer, which have not been observed in any polymeric system.

The self-assembly of (PS)(PI)(PFS) miktoarm star terpolymers (here, PFS is poly(ferrocenylethylmethylsilane)) was

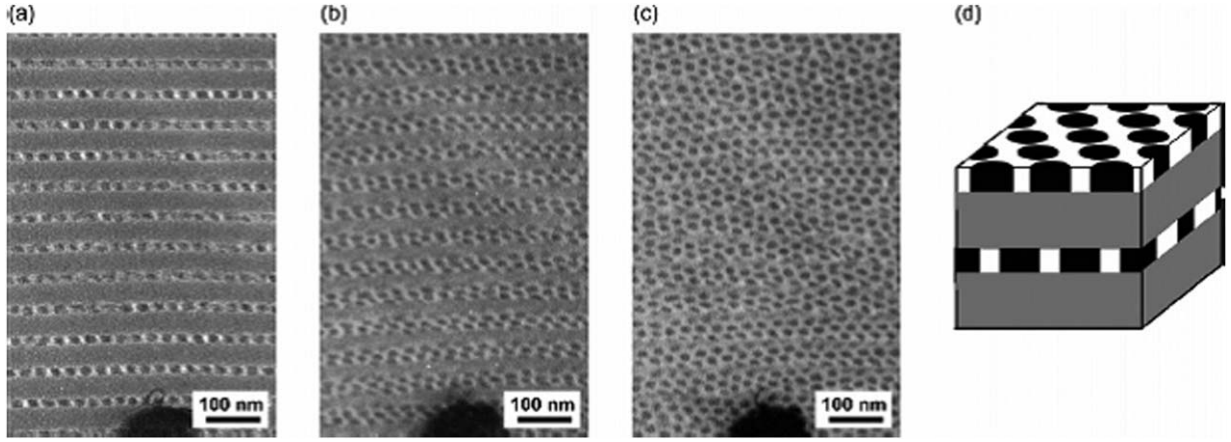

FIGURE 17 TEM images of a morphology for the (PS)(PI)(P2VP) miktoarm star terpolymer whose volume ratio of PS:PI:P2VP is 1.0:1.8:6.4 taken with tilt angles of (a) 0°, (b) 25°, and (c) 35° around a horizontal axis at the same sample location and the corresponding schematic (d). (Reproduced from ref. 78, with permission from American Chemical Society.)

studied by TEM.[35] Various morphologies were observed by varying the volume fraction of three arms in bulk films. Two different Archimedean tiling patterns, [8.8.4] and [12.6.4], and lamellae of PFS with alternating cylinders of PS and PI were found, which is generally consistent with the theoretical prediction.

Li et al.[83] investigated micellar morphologies of (PEO)(PE)(PF) miktoarm star terpolymer (here, PE is polyethylethylene; PF is poly(perfluoropropylene)) in a dilute aqueous solution. Since hydrophobic PE and lipophobic PF arms are superstrongly segregated, flat interfaces are obtained in micellar morphologies.[84,85] As a result, the micellar morphologies were tuned from discrete multicompartment micelles to extended wormlike structure depending on relative block lengths.

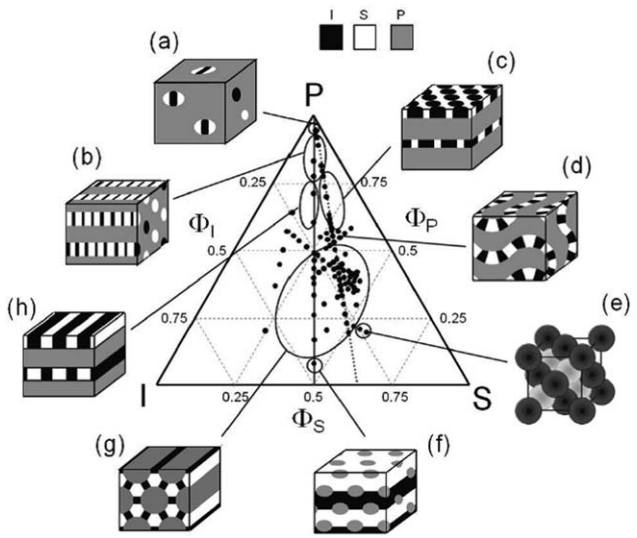

FIGURE 18 Kaleidoscopic morphologies from the (PS)(PI)(P2VP) miktoarm star terpolymer system. (a) Lamellae-in-sphere, (b) lamellae-in-cylinder, (c) cylinder-in-lamella, (d) hyperbolic tiling, (e) zinc blende, (f) sphere-sandwiched-with-lamella, (g) Archimedean tilting, and (h) lamellae-in-lamella. (Reproduced from ref. 33, with permission from IOP Publishing.)

Rod-Containing Miktoarm Star Copolymer

Rod-containing block copolymers have received great interest because of their structural asymmetry compared to conventional coil-b-coil block copolymers. Rod-coil linear block copolymers show unique morphologies such as the zigzag morphology[86] and mushroom-shaped microstructure.[87] However, relatively a few studies have been conducted focusing on the microphase separation for rod-containing miktoarm star copolymers, probably because of difficult synthesis. However, a recent development of synthetic methods can allow one to synthesize and characterize rod-containing miktoarm star copolymers.

Babin et al.[88] investigated the microdomain structures of A_2B miktoarm star copolymers composed of two poly(glutamic acid) (PGA) block and one PS block, where the PGA block adopted a rigid rod-like α-helical conformation. All miktoarm star copolymers have the hexagonal packing of PGA helices in lamellar structure independently of the composition, reflecting the strong strength of the rod–rod interaction and the high interaction parameter between the two blocks [Fig. 19(a)]. They also studied the effect of the macromolecular architecture on the organization of PGA α-helices. PGA can be folded or tilted depending on PGA content for linear diblock copolymers, whereas only stacked packing was observed in miktoarm star copolymer because two PGA arms in miktoarm star copolymers prevent the folding of the polypeptide segments [Fig. 1(b)].

Junnila et al.[89] investigated the morphologies of miktoarm star copolymers composed of PS block and rigid-like poly(ε-tert-butyloxycarbonyl-L-lysine) (PBLL) block. They found that PS_2PBLL miktoarm star copolymers formed lamellar morphologies with two different domain spacings.[86–88] In

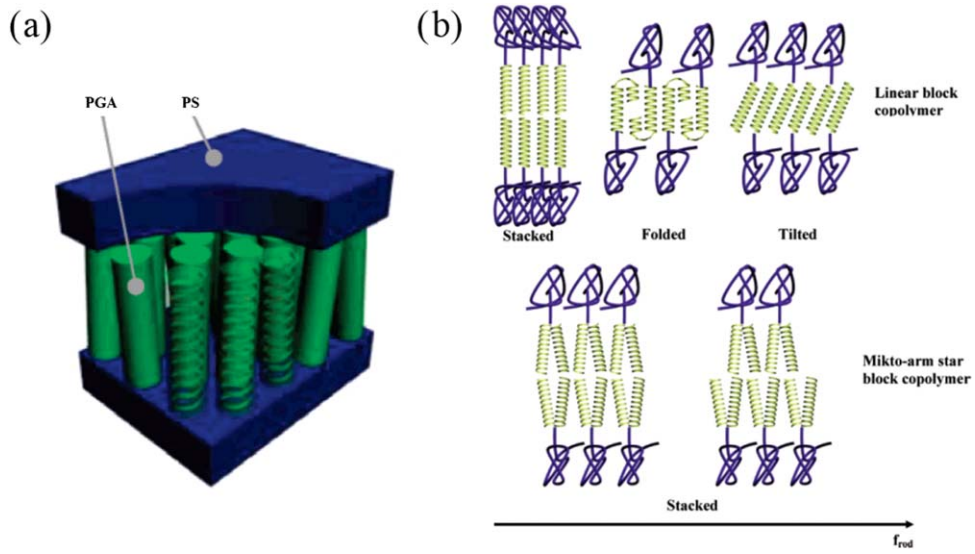

FIGURE 19 (a) Schematic representation for hexagonal packing of α-helix in lamellar morphology. (b) Schematic representation of the local packing of the PGA block as a function of the rod fraction for PS-*b*-PGA and $PS(PGA)_2$ miktoarm star copolymers.(Reproduced from ref. 88, with permission from American Chemical Society).

contrast, PS_2PBLL_2 miktoarm star copolymers formed uniform lamellar morphology with bilayer stacking of the α-helices because the frustration between the PBLL and PS arms is not large (Fig. 20).

Microphase separation of (PS)(PI)(poly(γ-benzyl-L-glutamate)[PBLG]) miktoarm star terpolymer (here, PBLG is poly(γ-benzyl-L-glutamate)) was investigated by X-ray scattering, solid state NMR, and TEM. Rod-like PBLG block which is hexagonally packed formed pure PBLG domains, whereas two amorphous PS and PI are partially mixed.[90] Junnila et al.[91] investigated the morphology of (PS)(PI)(PBLL) miktoarm star terpolymer. In contrast to (PS)(PI)(PBLG) miktoarm star terpolymer,[90] well-defined hierarchical microstructure was formed in the solid state. The PS and PI arms form lamellae, while PBLL arms are stacked to form pure polypeptide lamellae (Fig. 21). This hierarchical structure is only observed when the volume fraction of each block is highly asymmetric, or the interactions between arms are very different. Considering that the molecular weight of the arms is similar, this microstructure is caused by the aggregation of rod-like PBLL.

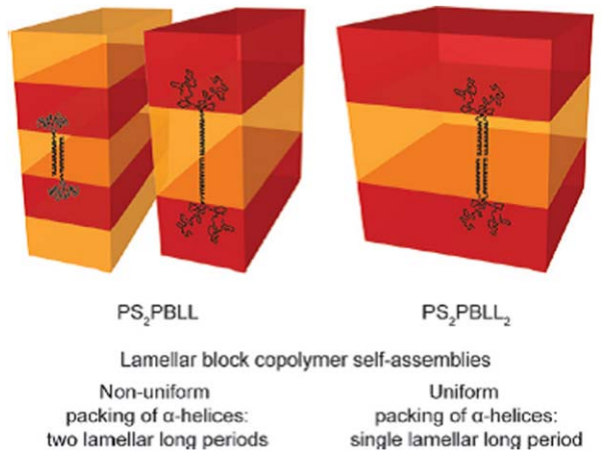

FIGURE 20 Schematic illustration of the packing of the miktoarm star copolymers in bulk. (Reproduced from ref. 89, with permission from American Chemical Society).

Goseki et al.[92] used A_2B miktoarm star copolymer composed of two PS coil and one polyhedral oligomeric silsesquioxane-containing poly(methacrylate) (PMAPOSS) and found that this exhibits cylindrical structure with the minor microdomains of the PMAPOSS due to higher curvature on the interface (Fig. 22). But, PMAPOSS cylindrical morphology was not observed in linear PS-*b*-PMAPOSS diblock copolymer because PMAPOSS molecule is bulky and crystalline, which makes PMAPOSS as rod-like segments. In addition, ellipsoidal cylinder-like morphology was observed, which is often observed in rod-containing diblock copolymers.[93,94]

Poly(3-alkylthiophene) (P3AT) is one of the most attractive π-conjugated polymers for organic field-effect transistors, organic photovoltaics, and chemical sensors. Several research groups studied the self-assembly of P3AT-containing linear block copolymers as nanoscale morphologies consisting of P3AT.[95] However, miktoarm star copolymers containing P3AT were rarely synthesized. Very recently, Park et al. prepared $(P3HT)_2PMMA$ miktoarm star copolymer with 48 wt.% of P3HT.[96] It shows nanofibril structure whose width is similar to that of P3HT-*b*-PMMA when the molecular weight of P3HT block is the same as one arm of P3HT in $(P3HT)_2PMMA$. This indicates that two P3HT backbones in each $(P3HT)_2PMMA$ could be stacked one by one along the

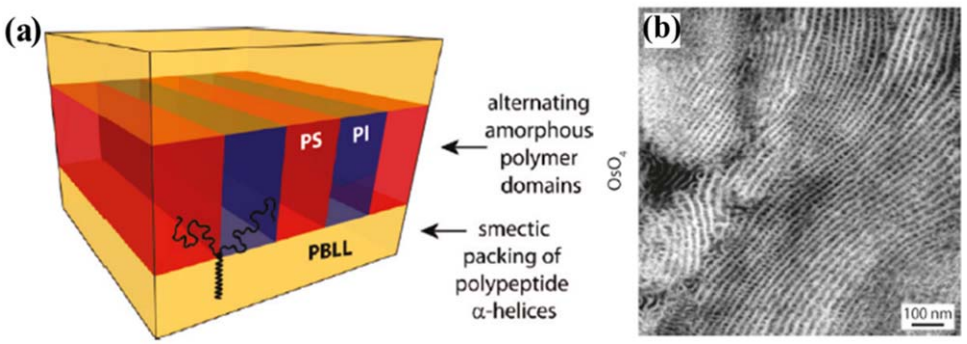

FIGURE 21 (a) Schematic illustration of the hierarchical structure of the (PS)(PI)(PBLL) miktoarm star copolymers in bulk. (b) TEM image of the miktoarm star copolymer annealed and stained with OsO_4 (PI dark, PS and PBLL light). (Reproduced from ref. 91, with permission from American Chemical Society).

nanofibril axis without any topological constraint because of strong π–π interaction between P3HT arms (Fig. 23). This morphology was also observed for thin film.

MORPHOLOGIES AND MICROPHASE SEPARATIONS OF STAR-SHAPED COPOLYMERS

Theory

The phase behavior of (B-*b*-A)$_n$ ($n = 1$, 3, 5, 9) star-shaped copolymers was predicted using SCFT simulation by Matsen and coworkers.[39,97] Simulation was performed using the standard Gaussian chain model with conformational symmetry between A (outer block) and B (inner block) segments. Cylindrical and spherical phases were expanded at A-rich volume fraction, as shown in Figure 24. This indicates that inner blocks are preferentially located inside the microdomain. Increasing number of arms (n) caused a shift of overall phase boundaries toward higher volume fraction of A block. Also, *Fddd* (O^{70}) region of star-shaped copolymer was greatly expanded compared with that of linear diblock copolymer.

Leibler predicted the phase separation critical point of symmetric diblock copolymer (f_A=0.5) containing N monomer units as $(\chi N)_c = 10.5$.[1] Cruz et al.[98] investigated the phase separation critical point behavior of (A-*b*-B)$_n$ star-shaped copolymers with volume fraction of A inner block. Inner A block monomers of star-shaped copolymer would be screened from interacting with B monomers as the number of arms (n) increases, which is different from diblock copolymer. This self-segregation causes different phase transitions,

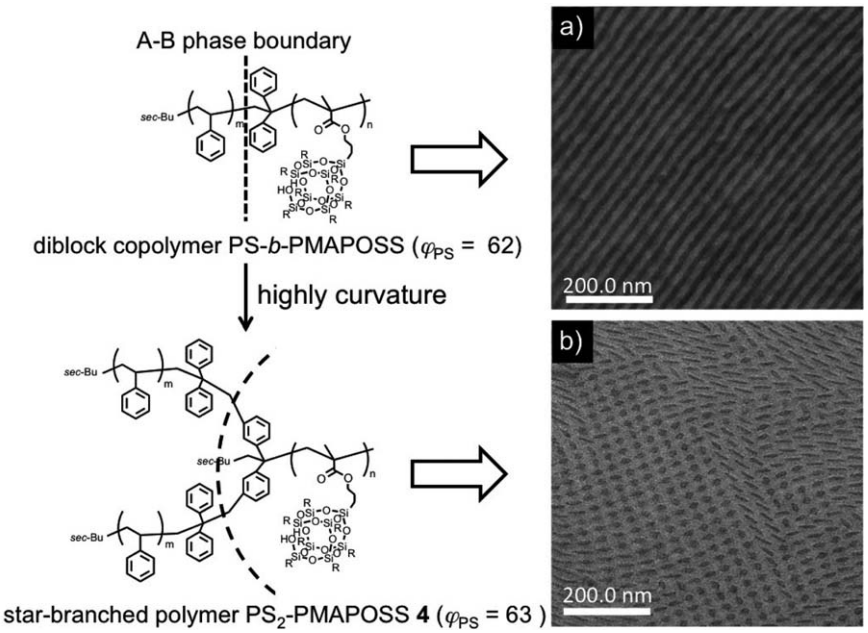

FIGURE 22 Differences between the morphology of (a) linear PS-*b*-PMAPOSS and (b) the PS_2PMAPOSS miktoarm star copolymer. The greater crowding on the PS side of the interface for the miktoarm star copolymer case leads to a high degree of curvature. (Reproduced from ref. 92, with permission from American Chemical Society.)

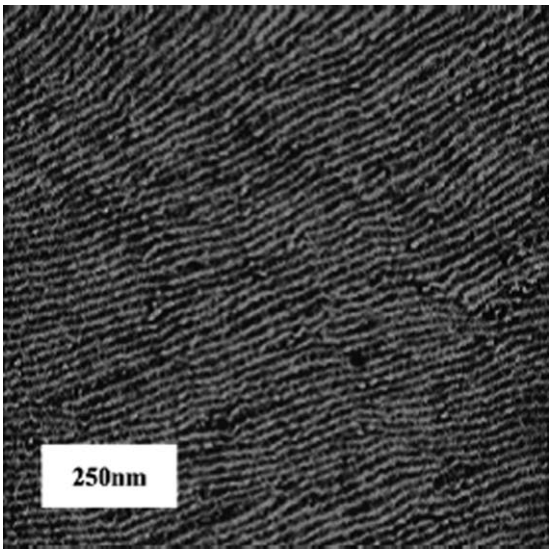

FIGURE 23 Tapping-mode AFM phase image of $(P3HT)_2PMMA$ miktoarm star copolymer film. (Reproduced from ref. 96, with permission from John Wiley and Sons)

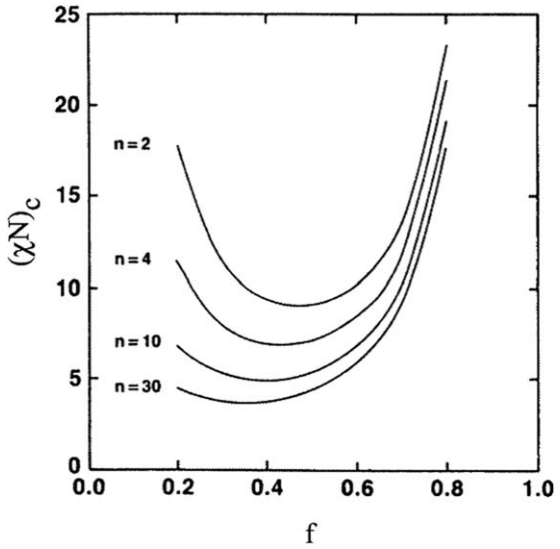

FIGURE 25 Variation of $(\chi N)_c$ with volume fraction of inner A block (f) for $(A\text{-}b\text{-}B)_n$ with various n. (Reproduced from ref. 98, with permission from American Chemical Society.)

as shown in Figure 25. Molecular architecture of star-shaped copolymer induced lower critical point of $(\chi N)_c$ and more asymmetric curves with increasing n. Recently, Lin and coworkers[99] explored the phase behavior of $(A\text{-}b\text{-}B)_{21}$ in bulk and under cylindrical confinement using the pseudo-spectral method of SCFT. They predicted an expanded disordered phase region, which means that it is more difficult to induce microphase separation of star-shaped copolymer compared with linear diblock copolymer. Also, the disordered region was expanded when the inner block had a larger volume fraction than the outer block.

Experimental of Star-Shaped Copolymers

Thomas and coworkers[100] explored the phase behavior of $(PI\text{-}b\text{-}PS)_n$ with PS outer block. The morphologies of a series of $(PI\text{-}b\text{-}PS)_{18}$ with various volume fractions of f_{PS} (0.09–0.91) were investigated in detail. They observed PS spheres, PS cylinders, PS double gyroid, lamellae, PI cylinders, and PI spheres with increasing f_{PS}, as shown in Figure 26. Because PI block was selectively stained by OsO_4 vapor, dark areas represent the PI phase. PS spherical and cylindrical microdomains were observed at minor volume fractions of the PS block, and reverse phase of PI spherical and cylindrical microdomains was found for major components of PS block. Interestingly, an ordered bicontinuous double gyroid (OBDG) was only observed when the minority component was the outer segment ($f_{PS} = 0.27$) as shown in Figure 27(a). But, cylindrical structure was exhibited when PS was inner block and minor volume fraction for $(PS\text{-}b\text{-}PI)_{18}$ with $f_{PS} = 0.27$. Of course, a reversed image contrast of OBDG structure was shown for $(PS\text{-}b\text{-}PI)_{18}$ with $f_{PI} = 0.27$ because the outer block was PI [Fig. 27(b)].

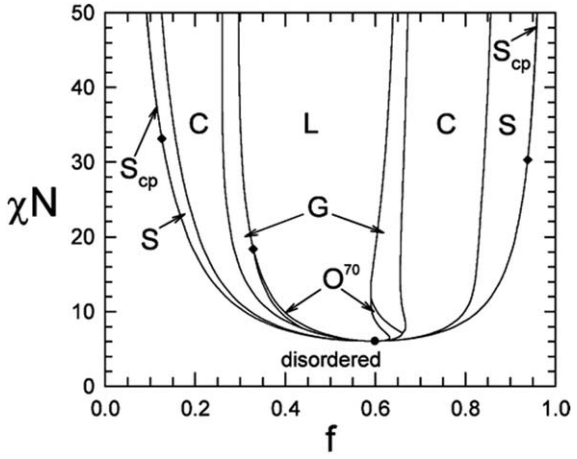

FIGURE 24 Phase diagram of $(B\text{-}b\text{-}A)_9$ depending on volume fraction of outer A block (f). Here N is the degree of polymerization of each diblock copolymer arm. (Reproduced from ref. 39, with permission from American Chemical Society.)

Also, they examined the effect of molecular weight and n on the transition of morphology of $(PI\text{-}b\text{-}PS)_n$ at fixed f_{PS} of 0.27.[101,102] Five different arms ($n = 2$, 4, 8, 12, 18) and three molecular weights of one arm (2.3×10^{-4}, 3.3×10^{-4}, 10×10^{-4} g/mol) were used. By increasing n or molecular weight of arms, the cylindrical microstructure was transformed to OBDG (Table 1). When they fixed the molecular weight of arms (2.3×10^4 g/mol), OBDG was observed for 18 arms, though the cylindrical structure showed up to 12 arms. Also, an OBDG was observed if the molecular weight of arms is increased from 2.3×10^4 g/mol to 3.3×10^4 g/mol at $n = 8$. Because of star-shaped molecular architecture, overcrowding of inner block (PI) is increased by increasing n. Thus, the conformational restriction for the inner block is increased. A phase transition from HEX to OBDG was observed at n larger than 6 when the molecular weight of one arm was fixed as 3.36×10^4 g/mol.[103] Moreover, at

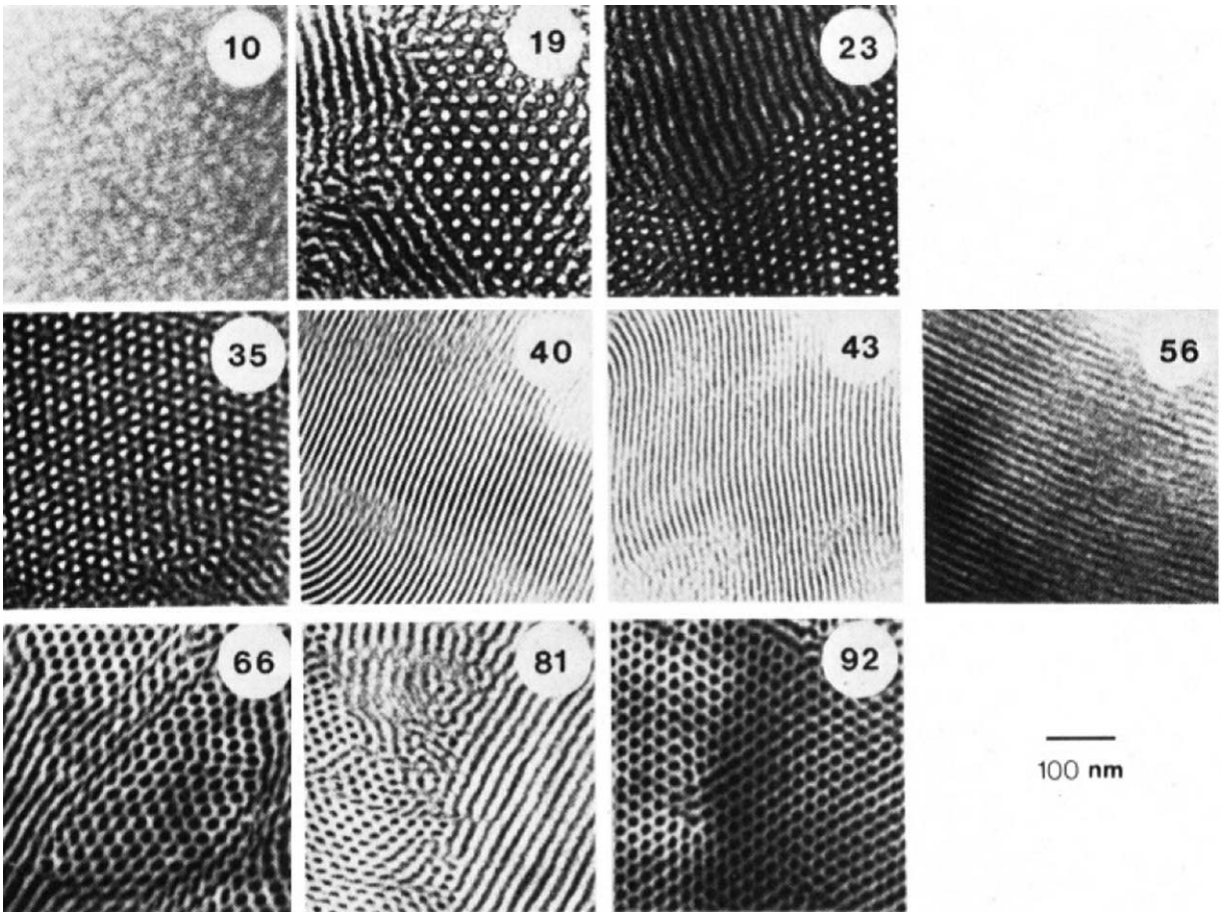

FIGURE 26 TEM images of (PI-*b*-PS)$_{18}$ labeled by volume fraction of PS outer block. (Reproduced from ref. 100, with permission from American Chemical Society.)

lower annealing temperature (120 °C), (PI-*b*-PS)$_6$ showed gyroid structure, while it showed HEX at 150 °C, and this transition is thermoreversible.

Uchida and coworkers[104–106] examined the morphologies of (PI-*b*-PS)$_n$ with high number of arms ($n = 26$ and 77) at a fixed volume fraction by SAXS and TEM. The dark part in Figure 28 corresponds to PI phases because of selective staining with OsO_4. Due to symmetric volume fraction of PI ($f_{PI} = 0.527$), lamellar structure was observed at all samples ($n = 2$, 26, and 77) even at $n = 77$ (Fig. 28). For number of arms of 16, 21, 26, and 16–19 wt % of PI block, all of (PI-*b*-

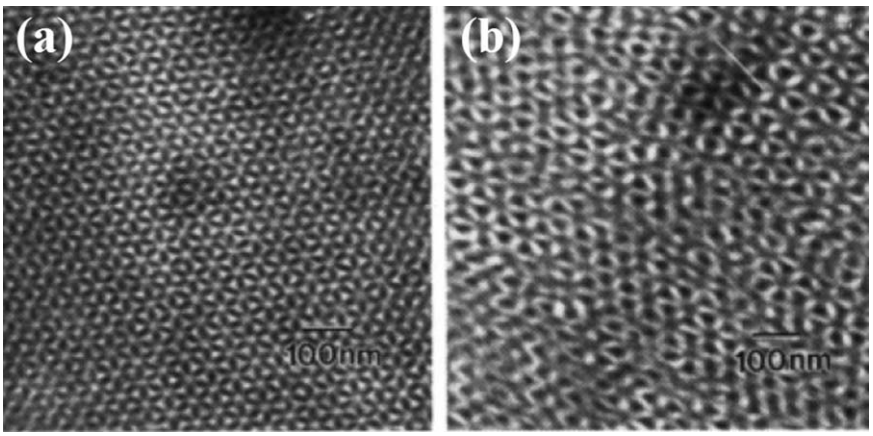

FIGURE 27 TEM images of (a) (PI-*b*-PS)$_{18}$ with outer PS block at $f_{PS} = 0.27$, (b) (PS-*b*-PI)$_{18}$ with outer PI block at $f_{PI} = 0.27$. (Reproduced from ref. 100, with permission from American Chemical Society.)

TABLE 1 Morphologies of (PI-*b*-PS)$_n$ Depending on the Molecular Weight of Arms and the Number of Arms.

Arm Molecular Weight	Arm Number				
	2	4	8	12	18
2.3×10^4	CYL	CYL	CYL	CYL	OBDG
3.3×10^4	CYL	CYL	OBDG	OBDG	OBDG
1.0×10^5		CYL		OBDG	OBDG

Reproduced with permission from ref. 101, with permission from American Chemical Society.

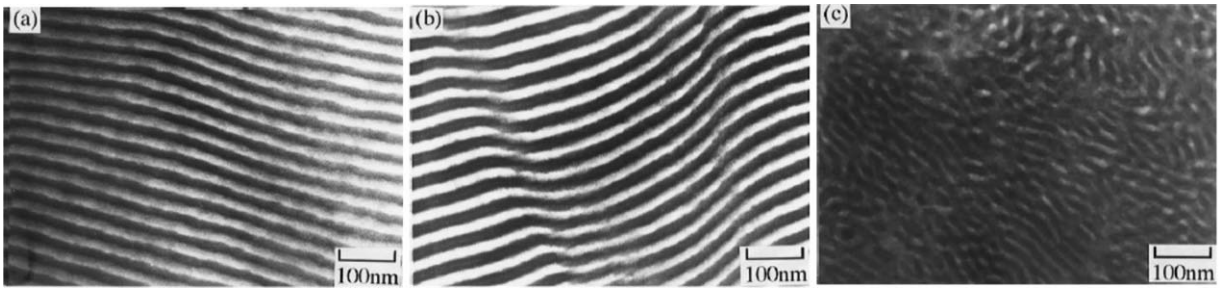

FIGURE 28 TEM images of (a) PI-*b*-PS, (b) (PI-*b*-PS)$_{26}$, and (c) (PI-*b*-PS)$_{77}$ with $f_{PI} = 0.527$. (Reproduced from ref. 106, with permission from Elsevier.)

PS)$_n$ showed face-centered cubic structure, which is the same as diblock copolymer.

Matsushita and coworkers[107] prepared (PI-*b*-PS)$_n$ ($n = 4$, 12) by an anionic polymerization technique and coupling reaction. After preparation of three kinds of linear PI-*b*-PS arms ($f_{PS} = 0.23$, 0.47, 0.78) by anionic polymerization, a coupling reaction followed to connect each arm by a linking agent. The same morphologies were observed between (PI-*b*-PS)$_n$ (after coupling) and corresponding linear PI-*b*-PS arms

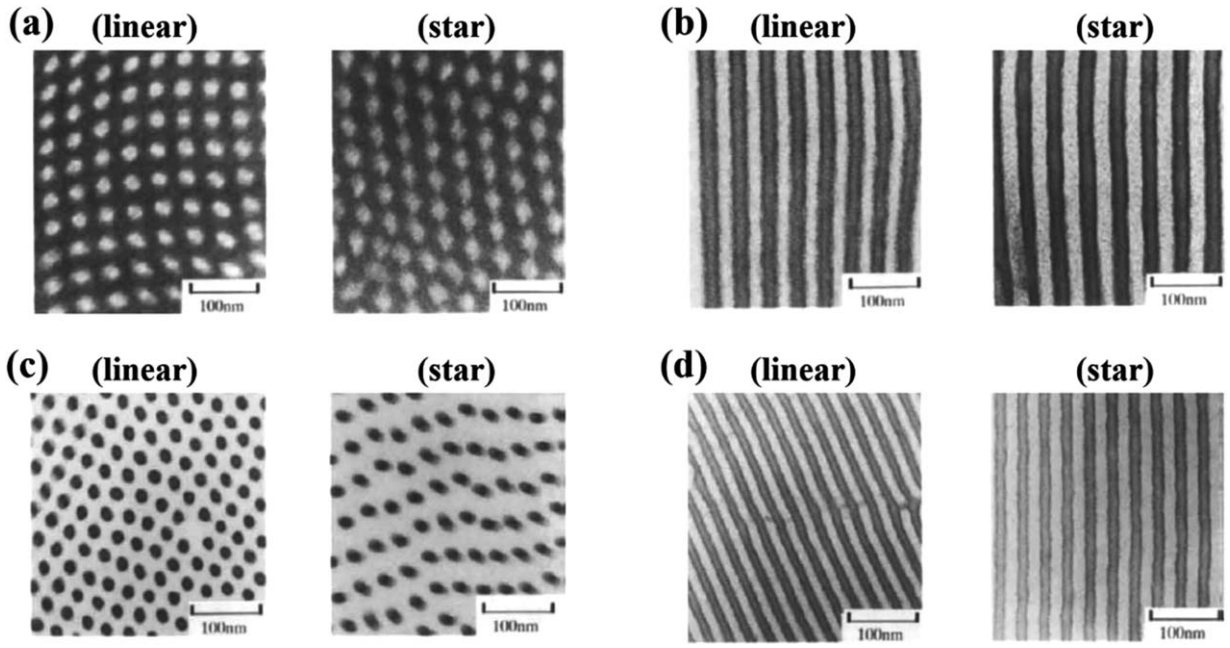

FIGURE 29 TEM images of (a) linear arm and (PI-*b*-PS)$_4$ with $f_{PS} = 0.23$, (b) linear arm and (PI-*b*-PS)$_4$ with $f_{PS} = 0.47$, (c) linear arm and (PI-*b*-PS)$_4$ with $f_{PS} = 0.78$, and (d) linear arm and (PI-*b*-PS)$_{12}$ with $f_{PS} = 0.47$. (Reproduced permission from ref. 107, with permission from Elsevier.)

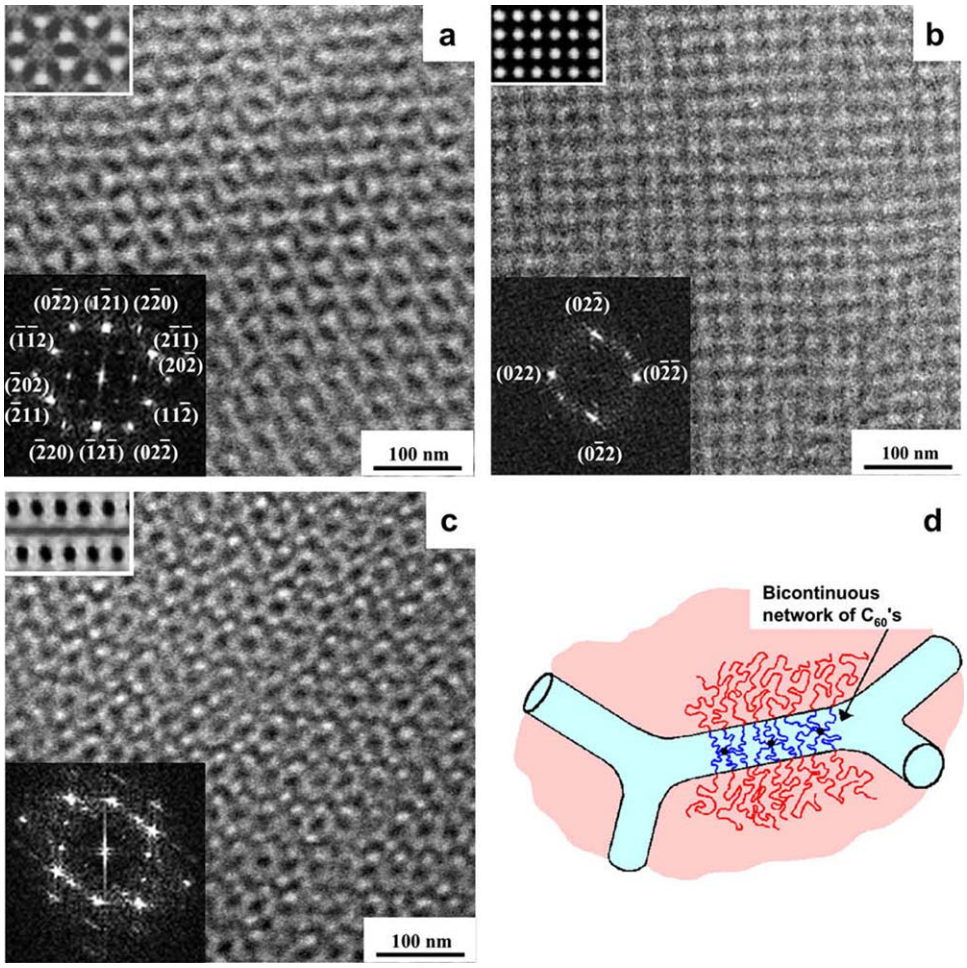

FIGURE 30 TEM projections of (PS-*b*-PI)$_6$ ($f_{PS} = 0.33$) with (a) 6-fold, (b) 4-fold, (c) 2-fold, and (d) schematic drawing of gyroid structure of PS network containing fullerene. (Reproduced from ref. 110, with permission from Elsevier).

(before coupling) irrespective of n as shown in Figure 29: PS cylinders ($f_{PS} = 0.23$), lamellae ($f_{PS} = 0.47$) and PI cylinders ($f_{PS} = 0.78$). For annealed films prepared using star-shaped copolymers and corresponding linear diblock copolymers, equal domain spacing was measured. These results suggest that the conformational entropy loss due to the molecular architecture of star-shaped copolymer may not be large enough to affect the morphology up to 12 arms.

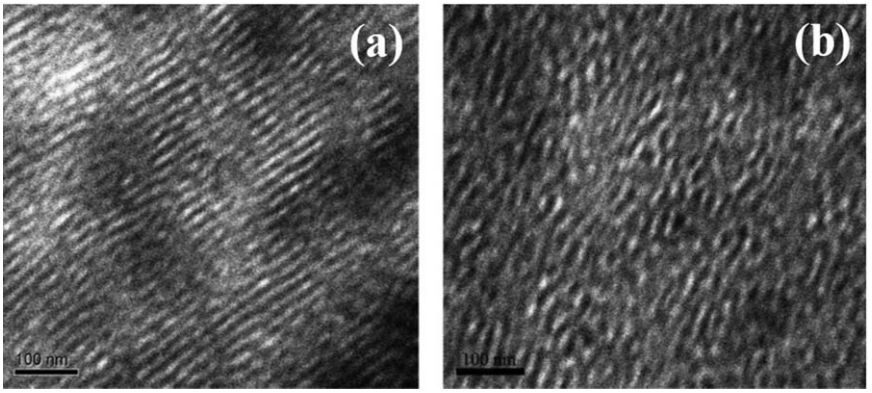

FIGURE 31 TEM image of (a) linear PS-*b*-PB-*b*-PS triblock copolymer and (b) (PB-*b*-PS)$_4$. (Reproduced from ref. 111, with permission from John Wiley and Sons.)

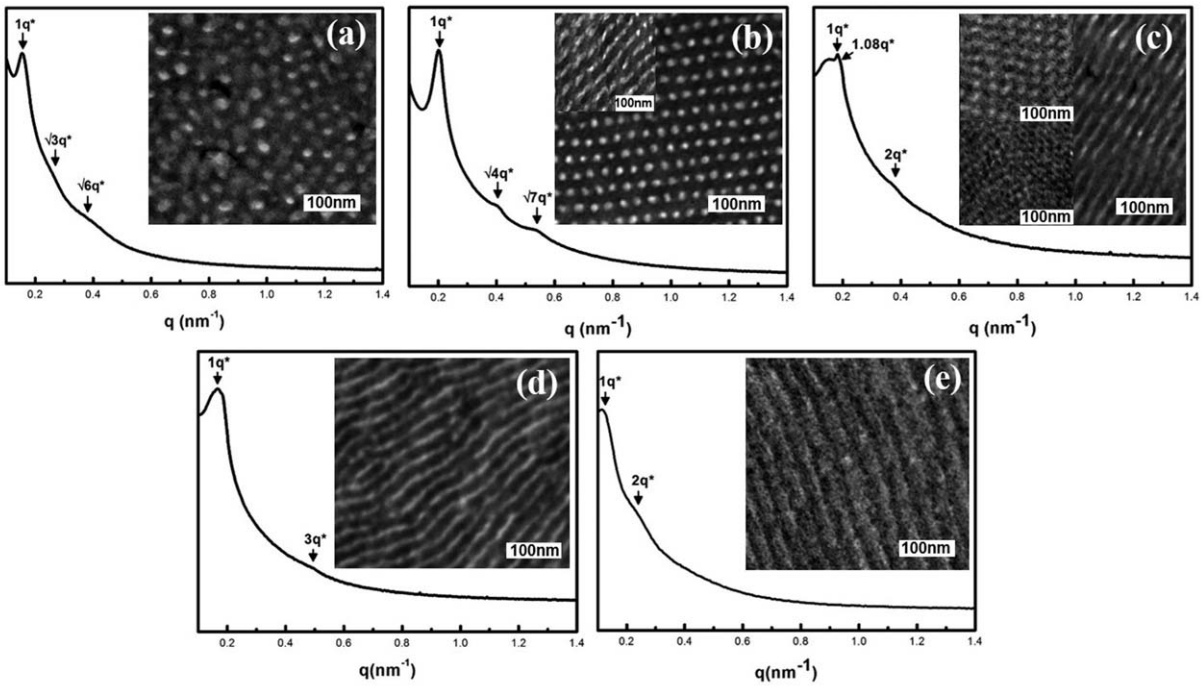

FIGURE 32 SAXS profiles and TEM images (insets) for the (PS-*b*-PMMA)$_{18}$ with different PMMA length. (a) $f_{PMMA} = 0.30$, (b) $f_{PMMA} = 0.38$, (c) $f_{PMMA} = 0.40$, (d) $f_{PMMA} = 0.48$, and (e) $f_{PMMA} = 0.77$. (Reproduced from ref. 112, with permission from American Chemical Society.)

Matyjaszewski and coworkers[108,109] prepared (PBA-*b*-PMMA)$_3$ with three different weight fractions of PMMA (13, 26, and 36 wt %.) by ATRP. Interestingly, a sample with 13 wt % of PMMA showed cylindrical structure. Also, they prepared (PBA-*b*-PMMA)$_n$ ($n = 10$, 20) with 27 wt % of PMMA. Significantly increased tensile strength and the elastic modulus was observed for (PBA-*b*-PMMA)$_n$ ($n = 10$, 20) compared with linear block copolymer and (PBA-*b*-PMMA)$_3$. This suggests that increased hard-domain interconnectivity between the star-shaped copolymer molecules improved tensile strength.

Brinkmann and coworkers[110] synthesized (PS-*b*-PI)$_6$ using a fullerene C_{60} as a core. After preparation of living PI-*b*-PS-Li^+ by anionic polymerization, C_{60} was subsequently added to graft polymer arms on C_{60}. Microstructures of PS cylinders ($f_{PS} = 0.22$), gyroid ($f_{PS} = 0.33$), lamellae ($f_{PS} = 0.46$), and PI cylinders ($f_{PS} = 0.77$) were observed by controlling the volume fraction of PS. They obtained gyroid structure although the inner block was the minority phase. As shown in Figure 30, 6-fold (a), 4-fold (b), and 2-fold (c) symmetries were observed, which are characteristic projections of gyroid. Because fullerene is used as junction point of star-shaped copolymer, assembly of fullerenes is possible within the PS microdomains, as shown in Figure 30(d).

Yu and coworkers[111] prepared linear PS-*b*-PB-*b*-PS triblock copolymer and (PB-*b*-PS)$_4$ with the same weight fraction of PS (40 wt %). Figure 31 presents the TEM images of linear and (PB-*b*-PS)$_4$. Lamellar microdomain was observed for linear PS-*b*-PB-*b*-PS triblock copolymer because of symmetric weight fraction [Fig. 31(a)], while sea-island morphology was exhibited for star-shaped copolymer [Fig. 31(b)].

Very recently, Kim and coworkers[112] prepared (PS-*b*-PMMA)$_{18}$ with various volume fractions of PMMA outer block (f_{PMMA}) using cyclodextrin as an initiator. The microdomains of (PS-*b*-PMMA)$_{18}$ changed from BCC, HEX, PL, and LAM with increasing f_{PMMA} from 0.3 to 0.8 (Fig. 32). Interestingly, (PS-*b*-PMMA)$_{18}$ with f_{PMMA} of 0.77 showed highly asymmetric lamellar microdomains, while the corresponding linear PS-*b*-PMMA diblock copolymer with the same volume fraction should not have lamellar microdomains. To analyze the arm information, the ester groups located between cyclodextrin and PS block were cut by hydrolysis. Spherical microdomains were observed after cutting of (PS-*b*-PMMA)$_{18}$ with $f_{PMMA} = 0.77$, which showed asymmetric lamellar microdomains for the star-shaped structure. This result suggests that the microdomains are highly affected by the molecular architecture of block copolymer.

Although many morphologies have been reported for diblock copolymers[86,87] or miktoarm star copolymers containing rod block,[92] there has been no reports on morphologies for rod-containing star-shaped copolymers. We expect that star-shaped copolymers containing rod block would show unexpected morphologies.

CONCLUSIONS AND OUTLOOK

We have discussed the self-assembly of two kinds of star copolymers: miktoarm star copolymers (A_mB_n and ABC

miktoarm star terpolymer) and star-shaped copolymers ($(A\text{-}b\text{-}B)_n$). The most studied miktoarm star copolymers are AB_m miktoarm star copolymers, where the boundary of each morphology is shifted to higher volume fraction of a single arm due to steric hindrance at the interface. Miktoarm (especially ABC miktoarm) star copolymers can have various morphologies such as Archimedean tiling patterns, because the junction points of ABC miktoarm star terpolymers usually lie in the line, not plane. Star-shaped copolymers ($(A\text{-}b\text{-}B)_n$) have an asymmetric phase diagram. Most experimental studies on morphology are focused on $(PI\text{-}b\text{-}PS)_n$. The effect of the number and molecular weight of arms caused enlarged OBDG phase boundary. Also, OBDG structures were mainly observed when the minority component was the outer block, and cylindrical structures were exhibited when the inner block has minor volume fraction. This is consistent with the theoretical prediction that a cylindrical structure is more stable when the minority component consists of the inner part. Except the above results, the experimentally observed self-assembled morphology of star-shaped copolymers was almost similar to that of linear block copolymers. Sea-island morphologies or dramatic phase shifts of star-shaped copolymers, which were not observable, have been shown recently using different species of star-shaped copolymers.

Well-defined star copolymers usually have been synthesized by anionic polymerization, which limits various polymers as arms.[113] Since a click reaction was successfully used to synthesize ABC miktoarm star terpolymers,[114,115] it would be the one of best methods to synthesize star copolymers with various arms. Also, the development of synthetic techniques, such as CRP, has made it possible to make diverse architectures. Based on advanced synthetic skills, one can synthesize more complex miktoarm architectures such as ABCDE miktoarm star copolymers or diverse species of star-shaped copolymers that could exhibit rich morphologies. Rigid-rod polymers, such as polypeptides and conjugated polymers, have also attracted much interest. However, there are few works on the self-assembly of star copolymers containing rigid-rod polymers. Also, there are few theories for rigid-rod containing miktoarm or star-shaped copolymers. We expect that these kinds of star copolymers could open a new era in self-assembly of block copolymers.

To use these fascinating morphologies of star copolymers in real applications such as nanotemplates for lithography and electronic devices with nano feature sizes, the self-assembled structure on thin films should be investigated. It is well known that many variables affect self-assembly of block copolymers in thin films, including film thickness and the interactions between polymers and the substrate or free surface, which induces very different morphologies of thin film from that of bulk.[116–118] We hope that new kinds of nanopatterns not attained from linear-shaped block copolymers could be possible when miktoarm or star-shape copolymers are used.

ACKNOWLEDGMENTS

This work was supported by the National Creative Research Initiative Program supported by the National Research Foundation of Korea (2013R1A3A2042196).

REFERENCES

1 L. Leibler, *Macromolecules* **1980**, *13*, 1602–1617.

2 F. S. Bates, G. H. Fredrickson, *Ann. Rev. Phys. Chem.* **1990**, *41*, 525–557.

3 T. Hashimoto, In Thermoplastic Elastomers; N. R. Legge, G. Holden, H. E. Schroeder, Eds.; Hanser: New York, **1987**.

4 (a) J. K. Kim, J. I. Lee, D. H. Lee, *Macromol. Res.* **2008**, *16*, 267–292. (b) J. K. Kim, S. Y. Yang, Y. Lee, Y. Kim, *Prog. Polym. Sci.* **2010**, 1325–1349.

5 Y. S. Kim, H. Han, Y. S. Kim, W. Lee, M. Alexe, S. G. Baik, J. K. Kim, *Nano Lett.*, **2010**, *10*, 2141–2146.

6 Y. S. Kim, Y. Kim, H. Han, S. Jesse, S. Hyun, W. Lee, S. V. Kalinin, J. K. Kim, *J. Mater. Chem. C* **2013**, *1*, 5299–5302.

7 A. Jo, W. Joo, W. H. Jin, H. Nam, J. K. Kim, *Nat. Nanotechnol.* **2009**, *4*, 727–731.

8 Y. J. Kang, J. J. Walish, T. Gorishnyy, E. L. Thomas, *Nat. Mater.* **2007**, *6*, 957–960.

9 S. Y. Yang, I. Ryu, H. Y. Kim, J. K. Kim, S. K. Jang, T. P. Russell, *Adv. Mater.* **2006**, *18*, 709–712.

10 S. Y. Yang, J. Park, J. Yoon, M. Ree, S. K. Jang, J. K. Kim, *Adv. Funct. Mater.* **2008**, *18*, 1371–1377.

11 J. I. Lee, S. H. Cho, S.-M. Park, J. K. Kim, H.-W. Yu, Y. C. Kim, T. P. Russell, *Nano Lett.* **2008**, *8*, 2315–2320.

12 S. Y. Yang, J.-A. Yang, E. S. Kim, G. Jeon, E. J. Oh, K. Y. Choi, S. K. Hahn, J. K. Kim, *ACS Nano* **2010**, *4*, 3817–3822.

13 W. J. Cho, Y. Kim, J. K. Kim, *ACS Nano* **2012**, *6*, 249–255.

14 S. H. Han, V. Pryamitsyn, D. S. Bae, J. H. Kwak, V. Ganesan, J. K. Kim, *ACS Nano* **2012**, *6*, 7966–7972.

15 J. Hahn, V. Filiz, S. Rangou, J. Clodt, A. Jung, K. Buhr, C. Abetz, V. Abetz, *J. Polym. Sci., Part B: Polym. Phys.* **2013**, *51*, 281–290.

16 S. Strandman, A. Zarembo, A. A. Darinskii, P. Laurinmaki, S. J. Butcher, E. Vuorimaa, H. Lemmetyinen, H. Tenhu, *Macromolecules* **2008**, *41*, 8855–8864.

17 M. Prabaharan, J. J. Grailer, S. Pilla, D. A. Steeber, S. Gong, *Biomaterials* **2009**, *30*, 5757–5766.

18 M. A. R. Meier, J-F. Gohy, C-A. Fustin, U. S. Schubert, *J. Am. Chem. Soc.* **2004**, *126*, 11517–112521.

19 X. Pang, L. Zhao, M. Akinc, J. K. Kim, Z. Lin, *Macromolecules* **2011**, *44*, 3746–3752.

20 X. Pang, L. Zhao, C. Feng, Z. Lin, *Macromolecules* **2011**, *44*, 7176–7183.

21 X. Pang, L. Zhao, W. Han, X. Xin, Z. Lin, *Nat. Nanotechnol.* **2013**, *8*, 426–431.

22 X. Pang, C. Feng, H. Xu, W. Han, X. Xin, H. Xia, F. Qiu, Z. Lin, *Polym. Chem.* **2014**, *5*, 2747–2755.

23 J. Xia, X. Zhang, K. Matyjaszewski, *Macromolecules* **1999**, *32*, 4482–4484.

24 X. Zhang, J. Xia, K. Matyjaszewski, *Macromolecules* **2000**, *33*, 2340–2345.

25 K.-Y. Baek, M. Kamigaito, M. Sawamoto, *Macromolecules* **2001**, *34*, 7629–7635.

26 J. Ueda, M. Kamigaito, M. Sawamoto, *Macromolecules* **1998**, *31*, 6762–6768.

27 K. Matyjaszewski, P. J. Miller, J. Pyun, G. Kickelbick, S. Diamanti, *Macromolecules* **1999**, *32*, 6526–6535.

28 M. Li, N. M. Jahed, K. Min, K. Matyjaszewski, *Macromolecules* **2004**, *37*, 2434–2441.

29 M. Pitsikalis, S. Pispas, J. W. Mays, N. Hadjichristidis, *Adv. Polm. Sci.* **1998**, *135*, 1–137.

30 K. Ishizu, U. Uchida, *Prog. Polym. Sci.* **1999**, *24*, 1439–1480.

31 N. Hadjichristidis, S. Pispas, M. Pitsikalis, H. Iatrou, C. Vlahos, *Adv. Polm. Sci.* **1999**, *142*, 71–127.

32 L-E. S. Cadena, M. Gauthier, *Polymers* **2010**, *2*, 596–622.

33 Y. Matsushita, K. Hayashida, T. Dotera, A. Takano, *J. Phys. Condens. Matter* **2011**, *23*, 284111.

34 K. Hayashida, T. Dotera, A. Takano, Y. Matsushita, *Phys. Rev. Lett* **2007**, *98*, 195502.

35 A. Nunns, C. A. Ross, I. Manners, *Macromolecules* **2013**, *46*, 2628–2635.

36 S. T. Milner, *Macromolecules* **1994**, *27*, 2333–2335.

37 G. Floudas, N. Hadjichristidis, Y. Tselikas, I. Erukhimovich, *Macromolecules* **1997**, *30*, 3090–3096.

38 G. M. Grason, R. D. Kamien, *Macromolecules* **2004**, *37*, 7371–7380.

39 M. W. Matsen, *Macromolecules* **2012**, *45*, 2161–2165.

40 T. S. Bailey, C. M. Hardy, T. H. Epss, *F. S. Bates Macromolecules* **2002**, *35*, 7007–7017.

41 C.-I. Huang, H.-T. Yu, *Polymer* **2007**, *48*, 4537–4546.

42 S. Pispas, A. Avgeropoulos, N. Hadjichristidis, J. Roovers, *J. Polym. Sci., Part B: Polym. Phys.* **1999**, *37*, 1329–1335.

43 T. Gemma, A. Hatano, T. Dotera, *Macromolecules* **2002**, *35*, 3225–3237.

44 X. He, L. Huang, H. Liang, C. Pan, *J. Chem. Phys.* **2003**, *118*, 9861–9863.

45 T. M. Birshtein, A. A. Polotsky, V. Abetz, *Macromol. Theory Simul.* **2004**, *13*, 512–519.

46 H. Hückstädt, T. Goldacker, A. Göpfert, V. Abetz, *Macromolecules* **2000**, *33*, 3757–3761.

47 C.-I. Huang, H.-K. Fang, C.-H. Lin, *Phys. Rev. E* **2008**, *77*, 031804.

48 Y. Xia, Z. Sun, T. Shi, J. Chen, L.An, Y. Jia, *Polymer* **2008**, *49*, 5596–5601.

49 Y. Xia, J. Chen, Z. Sun, T. Shi, L. An, Y. Jia, *J. Chem. Phys.* **2009**, *131*, 144905.

50 M.W. Matsen, C. Barrett, *J. Chem. Phys.* **1998**, *109*, 4108–4118.

51 V. Pryamitsyn, V. Ganesan, *J. Chem. Phys.* **2004**, *120*, 5824–5838.

52 N. Hadjichristidis, H. Iatrou, S. Behal, J. Chludzinski, M. Disko, R. Garner, K. Liang, D. Lohse, S. Milner, *Macromolecules* **1993**, *26*, 5812–5815.

53 K. Chrissopoulou, S. Harville, S. H. Anastasiadis, G. Fytas, J. W. Mays, N. Hadjichristidis, *J. Polym. Sci., Part B: Polym. Phys.* **1999**, *37*, 3385–3391.

54 Y. Tselikas, H. Iatrou, N. Hadjichristidis, K. S. Liang, K. Mohanty, D. J. Lohse, *J. Chem. Phys.* **1996**, *105*, 2456–2462.

55 Y. Tselikas, N. Hadjichristidis, R. L. Lescanec, C. C. Honeker, M. Wohlgemuth, E. L. Thomas, *Macromolecules* **1996**, *29*, 3390–3396.

56 D. J. Pochan, S. P. Gido, S. Pispas, J. W. Mays, *Macromolecules* **1996**, *29*, 5099–5105.

57 S. Sioula, Y. Tselikas, N. Hadjichristidis, *Macromol. Symp.* **1997**, *117*, 167–174.

58 L. Yang, S. Hong, S. P. Gido, G. Velis, N. Hadjichristidis, *Macromolecules* **2001**, *34*, 9069–9073.

59 A. Mavroudis, A. Avgeropoulos, N. Hadjichristidis, E. L. Thomas, D. Lohse, *J. Chem. Mater.* **2003**, *15*, 1976–1983.

60 T. Isono, I. Otsuka, Y. Kondo, S. Halila, S. B. Fort, C. Rochas, T. Satoh, R. Borsali, T. Kakuchi, *Macromolecules* **2013**, *46*, 1461–1469.

61 T. Isono, I. Otsuka, D. Suemasa, C. Rochas, T. Satoh, R. Borsali, T. Kakuchi, *Macromolecules* **2013**, *46*, 8932–8940.

62 F. L. Beyer, S. P. Gido, Y. Poulos, A. Avgeropoulos, N. Hadjichristidis, *Macromolecules* **1997**, *30*, 2373–2376.

63 C. Turner, N. Sheller, M. Foster, B. Lee, S. Corona-Galvan, R. Quirk, B. Annis, J.-S. Lin, *Macromolecules* **1998**, *31*, 4372–4375.

64 F. L. Beyer, S. P. Gido, D. Uhrig, J. W. Mays, N. B. Tan, S. F. Trevino. *J. Polym. Sci., Part B: Polym. Phys.* **1999**, *37*, 3392–3400.

65 M. W. Matsen, F. Bates, *Macromolecules* **1996**, *29*, 7641–7644.

66 Y. Zhu, S, P. Gido, M. Moshakou, H. Iatrou, N. Hadjichristidis, S. Park, T. Chang, *Macromolecules* **2003**, *36*, 5719–5724.

67 Y. Rho, C. Kim, T. Higashihara, S. Jin, J. Jung, T. J. Shin, A. Hirao, M. Ree, *ACS Macro Lett.* **2013**, *2*, 849–855.

68 A. Werner, G. H. Fredrickson, *J. Polym. Sci., Part B: Polym. Phys.* **1997**, *35*, 849–864.

69 S. Okamoto, H. Hasegawa, T. Hashimoto, T. Fujimoto, H. Zhang, T. Kazama, A. Takano, Y. Isono, *Polymer* **1997**, *38*, 5275–5281.

70 S. Sioula, N. Hadjichristidis, E. L. Thomas, *Macromolecules* **1998**, *31*, 5272–5277.

71 S. Sioula, N. Hadjichristidis, E. L. Thomas, *Macromolecules* **1998**, *31*, 8429–8432.

72 K. Yamauchi, K. Takahashi, H. Hasegawa, H. Iatrou, N. Hadjichristidis, T. Kaneko, Y. Nishikawa, H. Jinnai, T. Matsui, H. Nishioka, *Macromolecules* **2003**, *36*, 6962–6966.

73 H. Hückstädt, A. Göpfert, V. Abetz, *Macromol. Chem. Phys.* **2000**, *201*, 296–307.

74 A. Takano, S. Wada, S. Sato, T. Araki, K. Hirahara, T. Kazama, S. Kawahara, Y. Isono, A. Ohno, N. Tanaka, Y. Matsushita, *Macromolecules* **2004**, *37*, 9941–9946.

75 A. Takano, W. Kawashima, A. Noro, Y. Isono, N. Tanaka, T. Dotera, Y. Matsushita, *J. Polym. Sci., Part B: Polym. Phys.* **2005**, *43*, 2427–2432.

76 A. Takano, W. Kawashima, S. Wada, K. Hayashida, S. Sato, S. Kawahara, Y. Isono, M. Makihara, N. Tanaka, D. Kawaguchi, Y. Matsushita, *J. Polym. Sci., Part B: Polym. Phys.* **2007**, *45*, 2277–2283.

77 K. Hayashida, W. Kawashima, A. Takano, Y. Shinohara, Y. Amemiya, Y. Nozue, Y. Matsushita, *Macromolecules* **2006**, *39*, 4869–4872.

78 K. Hayashida, N. Saito, S. Arai, A. Takano, N. Tanaka, Y. Matsushita, *Macromolecules* **2007**, *40*, 3695–3699.

79 O. Ikkala, G. ten Brinke, *Science* **2002**, *295*, 2407–2409.

80 M. Muthukumar, C. K. Ober, E. L. Thomas, *Science* **1997**,*277*, 1225–1232.

81 J. Masuda, A. Takano, Y. Nagata, A. Noro, Y. Matsuhita, *Phys. Rev. Lett.* **2006**, *97*, 098301.

82 Y. Nagata, J. Masuda, A. Noro, D. Cho, A. Takano, Y. Matsushita, *Macromolecules* **2005**, *38*, 10220–10225.

83 Z. Li, E. Kesselman, Y. Talmon, M. A. Hillmayer, T. P. Lodge, *Science* **2004**, *306*, 98–101.

84 A. N. Semenov, L. A. Nyrkova, A. R. Khokhlov, *Macromolecules* **1995**, *28*, 7491–7500.

85 T. P. Lodge, M. A. Hillmyer, Z. Zhou, Y. Talmon, *Macromolecules* **2004**, *37*, 6680–6682.

86 J. Chen, E. L. Thomas, C. K. Ober, S.-P. Mao, *Science* **1996**, *273*, 343–346.

87 S. I. Stupp, V. LeBonheur, K. Walker, L.-S. Li, K. E. Huggins, M. Keser, A. Amstutz, *Science* **1997**, *276*, 384–389.

88 J. Babin, D. Taton, M. Brinkmann, S. Lecommandoux, *Macromolecules* **2008**, *41*, 1384–1392.

89 S. Junnila, N. Houbenov, A. Karatzas, N. Hadjichristidis, A. Hirao, H. Iatrou, O. Ikkala, *Macromolecules* **2012**, *45*, 2850–2856.

90 A. Gitsas, G. Floudas, M. Mondeshki, I. Lieberwirth, H. W. Spiess, H. Iatrou, N. Hadjichristidis, A. Hirao, *Macromolecules* **2010**, *43*, 1874–1881.

91 S. Junnila, N. Houbenov, S. Hanski, H. Iatrou, A. Hirao, N. Hadjichristidis, O. Ikkala, *Macromolecules* **2010**, *43*, 9071–9076.

92 R. Goseki, A. Hirao, M.-A. Kakimoto, T. Hayakawa, *ACS Macro Lett.* **2013**, *2*, 625–629.

93 B. D. Olsen, R. A. Segalman, *Macromolecules* **2007**, *40*, 6922–6929.

94 N. Sary, C. Brochon, G. Hadziioannou, R. Mezzenga, *Eur. Phys. J. E* **2007**, *24*, 379–384.

95 (a) H. C. Moon, A. Anthonysamy, Y. Lee, J. K. Kim, *Macromolecules* **2010**, *43*, 1747–1752. (b) H. C. Moon, A. Anthonysamy, J. K. Kim, A. Hirao, *Macromolecules* **2011**, *44*, 1894–1899. (c) H. C. Moon, D. Bae, J. K. Kim, *Macromolecules* **2012**, *45*, 5201–5207.

96 J. Park, H. C. Moon, J. K. Kim, *J. Polym. Sci., Part A: Polym. Chem.* **2013**, *51*, 2225–2232.

97 M. W. Matsen, M. Schick, *Macromolecules* **1994**, *27*, 6761–6767.

98 M. O. Cruz, I. C. Sanchez, *Macromolecules* **1986**, *19*, 2501–2508.

99 Y. Yu, W. Li, F. Qiu, Z. Lin, *Nanoscale* **2014**, *6*, 6844–6852.

100 D. S. Herman, D. J. Kinning, E. L. Thomas, L. J. Fetters, *Macromolecules* **1987**, *20*, 2940–2942.

101 D. B. Alward, D. J. Kinning, E. L. Thomas, L.J. Fetters, *Macromolecules* **1986**, *19*, 215–224.

102 D. J. Kinning, E. L. Thomas, D. B. Alward, L. J. Fetters, D. L. Handlin, Jr., *Macromolecules* **1986**, *19*, 1288–1290.

103 D. A. Hajduk, P. E. Harper, S. M. Gruner, C. C. Honeker, E. L. Thomas, L. J. Fetters, *Macromolecules* **1995**, *28*, 2570–2573.

104 K. Ishizu, S. Uchida, *Polymer* **1994**, *35*, 4712–4716.

105 K. Ishizu, S. Uchida, *J. Colloid Interface Sci.* **1995**, *175*, 296–296.

106 S. Uchida, A. Ichimura, K. Ishizu, *Polymer* **1999**, *40*, 1019–1023.

107 Y. Matsushita, T. Takasu, K. Yagi, K. Tomioka, I. Noda, *Polymer* **1993**, *35*, 2862–2866.

108 B. Dufour, K. Koynov, T. Pakula, K. Matyjaszewski, *Macromol. Chem. Phys.* **2008**, *209*, 1686–1693.

109 A. Nese, J. Mosnáček, A. Juhari, J. A. Yoon, K. Koynov, T. Kowalewski, K. Matyjaszewski, *Macromolecules* **2010**, *43*, 1227–1235.

110 B. Schmaltz, C. Mathis, M. Brinkmann, *Polymer* **2009**, *50*, 966–972.

111 M. Du, Q. Yu, Y. Lu, Q. Zheng, *J. Appl. Pol. Sci.* **2011**, *120*, 2962–2970.

112 S. Jang, H. C. Moon, J. Kwak, D. Bae, Y. Lee, J. K. Kim, *Macromolecules* **2014**, *47*, 5295–5302.

113 Y. Zhao, T. Higashihara, K. Sugiyama, A. Hirao, *J. Am. Chem. Soc.* **2005**, *127*, 14158–14159.

114 M. R. Whittaker, C. N. Urbani, M. J. Monteiro, *J. Am. Chem. Soc.* **2006**, *128*, 11360–11361.

115 K. Khanna, S. Varshney, A. Kakkar, *Macromolecules* **2010**, *43*, 5688–5698.

116 J. N. Albert, T. H. Epps, III, *Mater. Today* **2010**, *13*, 24–33.

117 M. Matsen, *J. Chem Phys.* **1997**, *106*, 7781–7791.

118 P. F. Green, R. Limary, *Adv. Colloid Interface Sci.* **2001**, *94*, 53–81.